Published for SISSA by Springer

Received: May 7, 2012
Accepted: June 5, 2012
Published: June 25, 2012

JHEP06(2012)141

Observation of double charm production involving open charm in pp collisions at $\sqrt{s} = 7$ TeV

The LHCb collaboration

Abstract: The production of J/ψ mesons accompanied by open charm, and of pairs of open charm hadrons are observed in pp collisions at a centre-of-mass energy of 7 TeV using an integrated luminosity of 355 pb^{-1} collected with the LHCb detector. Model independent measurements of absolute cross-sections are given together with ratios to the measured J/ψ and open charm cross-sections. The properties of these events are studied and compared to theoretical predictions.

Keywords: Hadron-Hadron Scattering

ArXiv ePrint: 1205.0975

doi:10.1007/JHEP06(2012)141

Contents

1 Introduction

Due to the high energy and luminosity of the LHC, charm production studies can be carried out in a new kinematic domain with unprecedented precision. As the cross-sections of open charm [1] and charmonium [2] production are large, the question of multiple production of these states in a single proton-proton collision naturally arises. Recently, studies of double charmonium and charmonium with associated open charm production have been proposed as probes of the quarkonium production mechanism [3]. In pp collisions, additional contributions from other mechanisms, such as Double Parton Scattering (DPS) [4–7] or the intrinsic charm content of the proton [8] to the total cross-section, are possible, though these constributions may not be mutually exclusive.

In this paper, both the production of J/ψ mesons together with an associated open charm hadron (either a D^0, D^+, D_s^+ or Λ_c^+)[1] and double open charm hadron production are studied in pp collisions at a centre-of-mass energy of 7 TeV. We denote the former process as J/ψ C and the latter as CC. In addition, as a control channel, $\mathrm{c\bar{c}}$ events where two open charm hadrons are reconstructed in the LHCb fiducial volume (denoted C$\overline{\text{C}}$) are studied.

[1]The inclusion of charge-conjugate modes is implied throughout this paper.

JHEP06(2012)141

While the production of $J/\psi\,C$ events have not been observed before in hadron interactions, evidence for the production of four charmed particles in pion-nuclear interactions has been reported by the WA75 collaboration [9].

Leading order (LO) calculations for the $gg \to J/\psi\,J/\psi$ process in perturbative QCD exist and give consistent results [10–12]. In the LHCb fiducial region ($2 < y_{J/\psi} < 4.5$, $p^{\rm T}_{J/\psi} < 10$ GeV/c), where $y_{J/\psi}$ and $p^{\rm T}_{J/\psi}$ stand for rapidity and transverse momentum respectively, the calculated $J/\psi\,J/\psi$ production cross-section is 4.1 ± 1.2 nb [12] in agreement with the measured value of $5.1 \pm 1.0 \pm 1.1$ nb [13]. Similar calculations for the $gg \to J/\psi\,c\bar{c}$ and $gg \to c\bar{c}c\bar{c}$ matrix elements exist [14, 15]. The calculated cross-sections for these processes in the acceptance region considered here ($2 < y_{J/\psi}, y_{\rm C} < 4$, $p^{\rm T}_{J/\psi} < 12$ GeV/c, $3 < p^{\rm T}_{\rm C} < 12$ GeV/c) are $\sigma\left(J/\psi\,{\rm C} + J/\psi\,\overline{\rm C}\right) \sim 18$ nb and $\sigma\left({\rm CC} + \overline{\rm CC}\right) \sim 100$ nb, where C stands for the open charm hadron. The predictions are summarized in table 1. These LO α_s^4 perturbative QCD results are affected by uncertainties originating from the selection of the scale for the α_s calculation that can amount to a factor of two.

The DPS contribution can be estimated, neglecting partonic correlations in the proton, as the product of the cross-sections of the sub-processes involved divided by an effective cross-section [4–7]

$$\sigma_{\rm DPS}\left({\rm C_1C_2}\right) = \begin{cases} \dfrac{1}{2}\dfrac{\sigma\left({\rm C_1}\right)\times\sigma\left({\rm C_1}\right)}{\sigma^{\rm DPS}_{\rm eff}}, & \text{for } {\rm C_1} = {\rm C_2} \\ \dfrac{\sigma\left({\rm C_1}\right)\times\sigma\left({\rm C_2}\right)}{\sigma^{\rm DPS}_{\rm eff}}, & \text{for } {\rm C_1} \neq {\rm C_2}. \end{cases} \tag{1.1}$$

Using this equation and the measured single charm cross-sections given in [1, 2] together with the effective cross-section measured in multi-jet events at the Tevatron $\sigma^{\rm DPS}_{\rm eff} = 14.5 \pm 1.7^{+1.7}_{-2.3}$ mb [16], the size of this contribution is estimated (see table 1). However, this approach has been criticized as being too naive [17].

Extra charm particles in the event can originate from the sea charm quarks of the interacting protons themselves. Estimates for the possible contribution in the fiducial volume used here are given in the appendix and summarized in table 1. It should be stressed that the charm parton density functions are not well known, nor are the $p^{\rm T}$ distributions of the resulting charm particles, so these calculations should be considered as upper estimates.

2 The LHCb detector and dataset

The LHCb detector [19] is a single-arm forward spectrometer covering the pseudorapidity range $2 < \eta < 5$, and is designed for the study of particles containing b or c quarks. The detector includes a high precision tracking system consisting of a silicon-strip vertex detector surrounding the proton-proton interaction region, a large-area silicon-strip detector located upstream of a dipole magnet with a bending power of about 4 Tm, and three stations of silicon-strip detectors and straw drift tubes placed downstream. The combined tracking system has a momentum resolution $\Delta p/p$ that varies from 0.4% at 5 GeV/c to 0.6% at 100 GeV/c, and an impact parameter resolution of 20 µm for tracks with high transverse momentum. Charged hadrons are identified using two ring-imaging Cherenkov (RICH)

JHEP06(2012)141

Mode	σ_{gg} [14, 15]	σ_{gg} [18]	σ_{DPS}	σ_{sea}
		[nb]		
$J/\psi D^0$	10 ± 6	7.4 ± 3.7	146 ± 39	220
$J/\psi D^+$	5 ± 3	2.6 ± 1.3	60 ± 17	100
$J/\psi D_s^+$	1.0 ± 0.8	1.5 ± 0.7	24 ± 7	30
$J/\psi \Lambda_c^+$	0.8 ± 0.5	0.9 ± 0.5	56 ± 22	
		[μb]		
D^0D^0			2.0 ± 0.5	1.5
D^0D^+			1.7 ± 0.4	1.4
$D^0D_s^+$			0.65 ± 0.15	0.4
$D^0\Lambda_c^+$			1.5 ± 0.5	
D^+D^+			0.34 ± 0.09	0.3
$D^+D_s^+$			0.27 ± 0.07	0.2
$D^+\Lambda_c^+$			0.64 ± 0.23	

Table 1. Estimates for the production cross-sections of the $J/\psi C$ and CC modes in the LHCb fiducial range given by the leading order $gg \to J/\psi c\bar{c}$ matrix element, σ_{gg} [14, 15, 18], the double parton scattering approach, σ_{DPS} and the sea charm quarks from the interacting protons, σ_{sea}.

detectors. Photon, electron and hadron candidates are identified by a calorimeter system consisting of scintillating-pad and pre-shower detectors, and electromagnetic and hadronic calorimeters. Muons are identified by a muon system composed of alternating layers of iron and multiwire proportional chambers. The trigger consists of a hardware stage based on information from the calorimeter and muon systems, followed by a software stage which applies a full event reconstruction.

Events with a $J/\psi \to \mu^+\mu^-$ final state are triggered using two hardware trigger decisions: the single-muon decision, which requires one muon candidate with a transverse momentum p^{T} larger than 1.5 GeV/c, and the di-muon decision, which requires two muon candidates with transverse momenta p_1^{T} and p_2^{T} satisfying the relation $\sqrt{p_1^{\mathrm{T}} \cdot p_2^{\mathrm{T}}} > 1.3$ GeV/c. The di-muon trigger decision in the software trigger requires muon pairs of opposite charge with $p^{\mathrm{T}} > 500$ MeV/c, forming a common vertex and with an invariant mass $2.97 < m_{\mu^+\mu^-} < 3.21$ GeV/c^2. Events with purely hadronic final states are accepted by the hardware trigger if there is a calorimeter cluster with transverse energy $E^{\mathrm{T}} > 3.6$ GeV. The software trigger decisions select generic displaced vertices from tracks with large χ^2 of impact parameter with respect to all primary pp interaction vertices in the event, providing high efficiency for purely hadronic decays [20].

To prevent a few events with high occupancy from dominating the CPU time in the software trigger, a set of global event cuts is applied on the hit multiplicities of each subdetector used by the pattern recognition algorithms. These cuts were chosen to reject events with a large number of pile-up interactions with minimal loss of data.

JHEP06(2012)141

The data used for this analysis comprises 355 ± 13 pb^{-1} of pp collisions at a centre-of-mass energy of $\sqrt{s} = 7$ TeV collected by the LHCb experiment in the first half of the 2011 data-taking period. Simulation samples used are based on the Pythia 6.4 generator [21] configured with the parameters detailed in ref. [22]. The EvtGen [23] and Geant4 [24] packages are used to describe hadron decays and for the detector simulation, respectively. The prompt charmonium production is simulated in Pythia according to the leading-order colour-singlet and colour-octet mechanisms.

3 Event selection

To select events containing multiple charm hadrons, first J/ψ, D^0, D^+, D_s^+ and Λ_c^+ candidates are formed from charged tracks reconstructed in the spectrometer. Subsequently, these candidates are combined to form J/ψ C, CC and C$\overline{\mathrm{C}}$ candidates.

Well reconstructed tracks are selected for these studies by requiring that the χ^2_{tr} provided by the track fit satisfy $\chi^2_{\mathrm{tr}}/\mathrm{ndf} < 5$, where ndf represents the number of degrees of freedom in the fit, and that the transverse momentum is greater than 650 (250) MeV/c for each muon (hadron) candidate. For each track, the global likelihoods of the muon and hadron hypotheses provided by reconstruction of the muon system are evaluated, and well identified muons are selected by a requirement on the difference in likelihoods $\Delta \ln \mathcal{L}_{\mu/\mathrm{h}} > 0$.

Good quality particle identification by the ring-imaging Cherenkov detectors is ensured by requiring the momentum of the hadron candidate to be between 3.2 GeV/c (10 GeV/c for protons) and 100 GeV/c, and the pseudorapidity to be in the range $2 < \eta < 5$. To select kaons (pions) the corresponding difference in logarithms of the global likelihood of the kaon (pion) hypothesis provided by the RICH system with respect to the pion (kaon) hypothesis, $\Delta \ln \mathcal{L}_{\mathrm{K}/\pi}$ ($\Delta \ln \mathcal{L}_{\pi/\mathrm{K}}$), is required to be greater than 2. For protons, the differences in logarithms of the global likelihood of the proton hypothesis provided by the RICH system with respect to the pion and kaon hypotheses, are required to be $\Delta \ln \mathcal{L}_{\mathrm{p}/\pi} > 10$ and $\Delta \ln \mathcal{L}_{\mathrm{p}/\mathrm{K}} > 10$, respectively.

Pions, kaons and protons, used for the reconstruction of long-lived charm particles, are required to be inconsistent with being produced in a pp interaction vertex. Only particles with a minimal value of impact parameter χ^2 with respect to any reconstructed proton-proton collision vertex $\chi^2_{\mathrm{IP}} > 9$, are considered for subsequent analysis. These selection criteria are summarized in table 2.

The selected charged particles are combined to form J/$\psi \to \mu^+\mu^-$, $\mathrm{D}^0 \to \mathrm{K}^-\pi^+$, $\mathrm{D}^+ \to \mathrm{K}^-\pi^+\pi^+$, $\mathrm{D}_\mathrm{s}^+ \to \mathrm{K}^-\mathrm{K}^+\pi^+$ and $\Lambda_\mathrm{c}^+ \to \mathrm{pK}^-\pi^+$ candidates. A vertex fit is made to all combinations and a selection criterion on the corresponding χ^2_{VX} applied. The transverse momentum, p^{T}, for open charm hadron candidates is required to be larger than 3 GeV/c. To ensure that the long-lived charm particle originates from a primary vertex, the minimal value of the charm particle's χ^2_{IP} with respect to any of the reconstructed proton-proton collision vertices is required to be < 9. In addition, the decay time $c\tau$ of long-lived charm mesons is required to be in excess of 100 μm, and in the range $100 < c\tau < 500$ μm for Λ_c^+ candidates. To suppress the higher combinatorial background for Λ_c^+ candidates, only pions, kaons and protons with a transverse momentum in excess of 0.5 GeV/c are used in this case.

JHEP06(2012)141

Track selection	
$\mu^\pm, h^\pm$	$\chi^2_{\rm tr}/{\rm ndf} < 5$
$\mu^\pm$	$p^{\rm T} > 650$ MeV/c
$h^\pm$	$p^{\rm T} > 250$ MeV/c & $2 < \eta < 5$ & $\chi^2_{\rm IP} > 9$
$\pi^\pm, K^\pm$	$3.2 < p < 100$ GeV/c
$p^\pm$	$10 < p < 100$ GeV/c
Particle identification	
$\mu^\pm$	$\Delta \ln \mathcal{L}_{\mu/h} > 0$
$\pi^\pm$	$\Delta \ln \mathcal{L}_{\pi/K} > 2$
$K^\pm$	$\Delta \ln \mathcal{L}_{K/\pi} > 2$
$p, \bar{p}$	$\Delta \ln \mathcal{L}_{p/K} > 10$ & $\Delta \ln \mathcal{L}_{p/\pi} > 10$

Table 2. Selection criteria for charged particles used for the reconstruction of charm hadrons.

		J/ψ $\mu^+\mu^-$	D^0 $K^-\pi^+$	D^+ $K^-\pi^+\pi^+$	D_s^+ $(K^+K^-)_\phi\,\pi^+$	Λ_c^+ $pK^-\pi^+$
y		$2 < y < 4$	$2 < y < 4$	$2 < y < 4$	$2 < y < 4$	$2 < y < 4$
$p^{\rm T}$	[GeV/c]	< 12	$3 < p^{\rm T} < 12$	$3 < p^{\rm T} < 12$	$3 < p^{\rm T} < 12$	$3 < p^{\rm T} < 12$
$\chi^2_{\rm VX}$		< 20	< 9	< 25	< 25	< 25
$\chi^2_{\rm IP}$		—	< 9	< 9	< 9	< 9
$\chi^2_{\rm fit}/{\rm ndf}$		< 5	< 5	< 5	< 5	< 5
$c\tau$	[μm]	—	$c\tau > 100$	$c\tau > 100$	$c\tau > 100$	$c\tau > 100$ $c\tau < 500$
$\lvert\cos\theta^*\rvert$		—	< 0.9	—	—	—
$m_{K^+K^-}$	[GeV/c^2]	—	—	—	< 1.04	—
$\min p^{\rm T}_{h^\pm}$	[GeV/c]	—	—	—	—	> 0.5

Table 3. Criteria used for the selection of charm hadrons.

A global decay chain fit of the selected candidates is performed [25]. For channels containing a J/ψ meson it is required that the muons be consistent with originating from a common vertex and that this be compatible with one of the reconstructed pp collision vertices. In the case of long-lived charm hadrons, the momentum direction is required to be consistent with the flight direction calculated from the locations of the primary and secondary vertices. To remove background from b-hadron decays the reduced χ^2 of this fit, $\chi^2_{\rm fit}/{\rm ndf}$, is required to be < 5. To further reduce the combinatorial background as well as cross-feed due to particle misidentification, for the decay mode $D^0 \to K^-\pi^+$ a selection criterion on the cosine of the angle between the kaon momentum in the D^0 centre-of-mass frame and the D^0 flight direction in the laboratory frame, θ^* is applied. For $D_s^+ \to K^+K^-\pi^+$ candidates, the invariant mass of the K^+K^- system is required to be consistent with the ϕ meson mass. These selection criteria are summarized in table 3.

JHEP06(2012)141

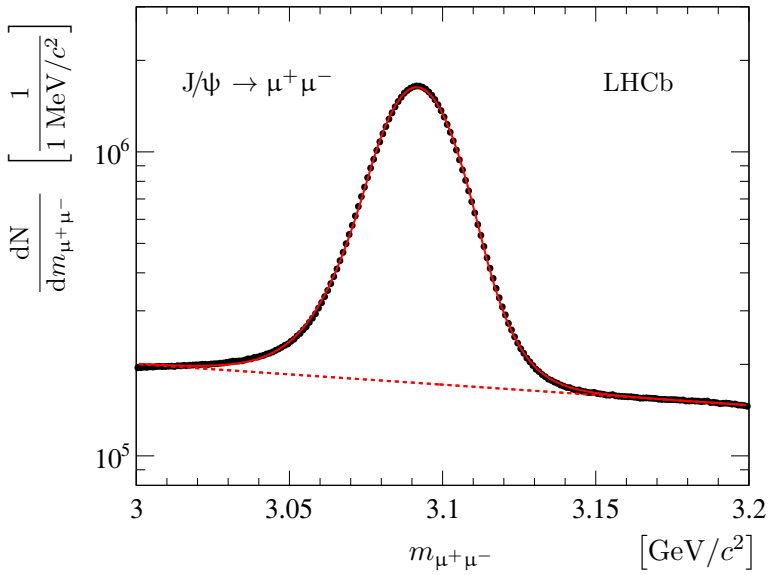

Figure 1. Invariant mass distribution for selected J/ψ candidates. The results of a fit to the model described in the text is superimposed on a logarithmic scale. The solid line corresponds to the total fitted PDF whilst the dotted line corresponds to the background component.

		J/ψ $\mu^+\mu^-$	D^0 $K^-\pi^+$	D^+ $K^-\pi^+\pi^+$	D_s^+ $(K^+K^-)_\phi\,\pi^+$	Λ_c^+ $pK^-\pi^+$
S	$[10^6]$	49.57	65.77	33.25	3.59	0.637
f_b^{MC}	[%]	1.6	1.7	1.3	2.6	4.5

Table 4. Yields, S, and contamination from b-hadron decays, f_b^{MC}, for the prompt charm signal.

The invariant mass distributions for selected J/ψ, D^0, D^+, D_s^+ and Λ_c^+ candidates are presented in figures 1 and 2 for J/ψ and open charm mesons, respectively. The distributions are modelled by a double-sided Crystal Ball function [13, 26] for the $J/\psi \to \mu^+\mu^-$, and a modified Novosibirsk function [27] for the $D^0 \to K^-\pi^+$, $D^+ \to K^-\pi^+\pi^+$ and $D_s^+ \to K^+K^-\pi^+$ and $\Lambda_c^+ \to pK^-\pi^+$ signals. In each case the combinatorial background component is modelled with an exponential function. The signal yields are summarized in table 4 together with an estimate of the contamination from the decays of b hadrons, f_b^{MC}. The latter has been estimated using simulated events, normalized to the corresponding measured cross-sections.

The selected charm candidates are paired to form di-charm candidates: J/ψ C, CC and $C\overline{C}$. A global fit of the di-charm candidates is performed [25], similar to that described above for single charm hadrons, which requires both hadrons to be consistent with originating from a common vertex. The reduced χ^2 of this fit, $\chi^2_{\rm global}/{\rm ndf}$, is required to be less than 5. This reduces the background from the pile-up of two interactions each producing a charm hadron to a negligible level. The remaining contamination from the pile-up and decays from beauty hadrons is extracted directly from the data as follows. The distribu-

JHEP06(2012)141

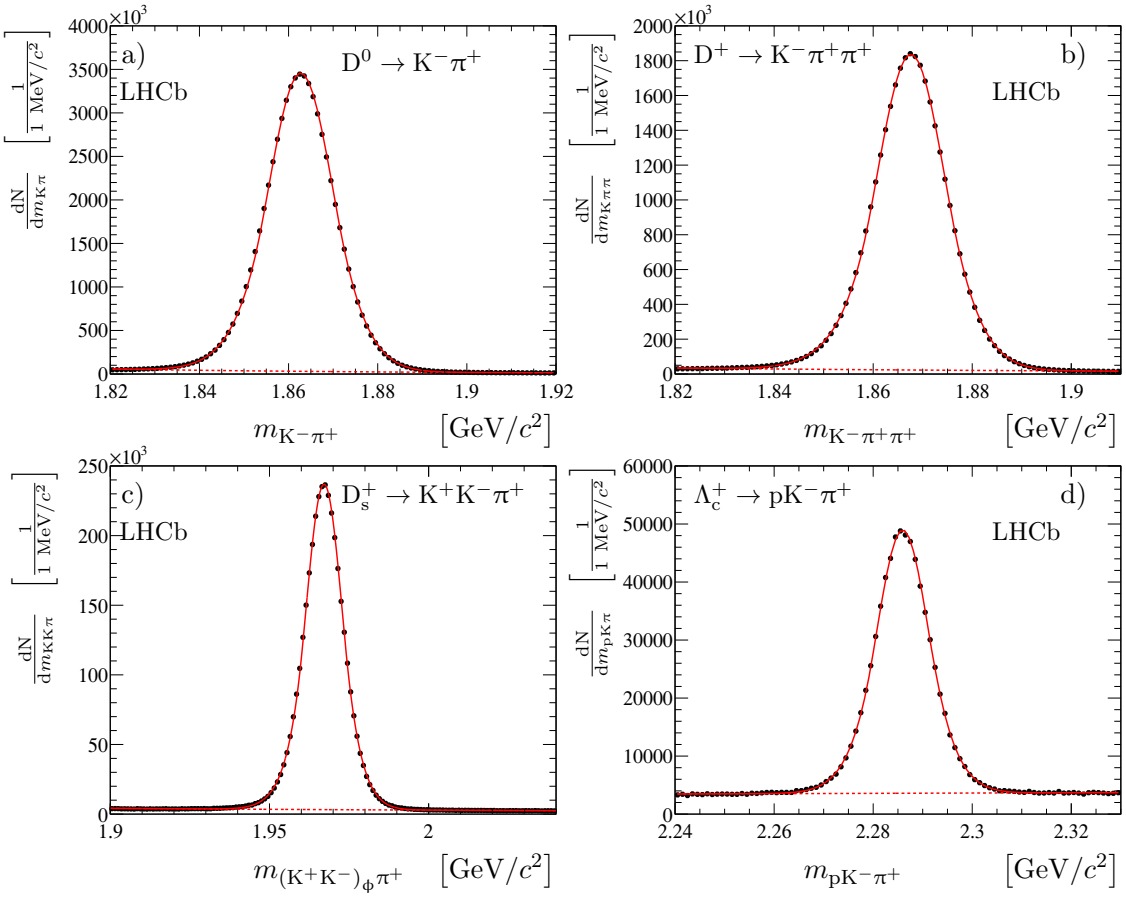

Figure 2. Invariant mass distributions for selected a) D^0, b) D^+, c) D_s^+ and d) Λ_c^+ candidates. The solid line corresponds to the total fitted PDF whilst the dotted line shows the background component.

tions of $\chi^2_{\text{global}}/\text{ndf}$ for $J/\psi\,D^0$, D^0D^0 and $D^0\overline{D}{}^0$ events are shown in figure 3. For the region $\chi^2_{\text{global}}/\text{ndf} > 5$ the distributions are well described by functions of the form[2]

$$f(x) \propto (\alpha x)^{\frac{n}{2}-1} e^{-\frac{\alpha x}{2}}, \tag{3.1}$$

where α and n are free parameters. Fits with this functional form are used to extrapolate the yield in the region $\chi^2_{\text{global}}/\text{ndf} > 5$ to the region $\chi^2_{\text{global}}/\text{ndf} < 5$. Based on these studies we conclude that background from pile-up is negligible.

The mass distributions for all pairs after these criteria are applied are shown in figures 4 to 8 for channels with sufficiently large data samples.

4 Signal determination

The event yields are determined using unbinned extended maximum likelihood fits to the mass distributions of the di-charm sample. The fit model is based on the probability

[2]The functional form is inspired by the χ^2 distribution.

JHEP06(2012)141

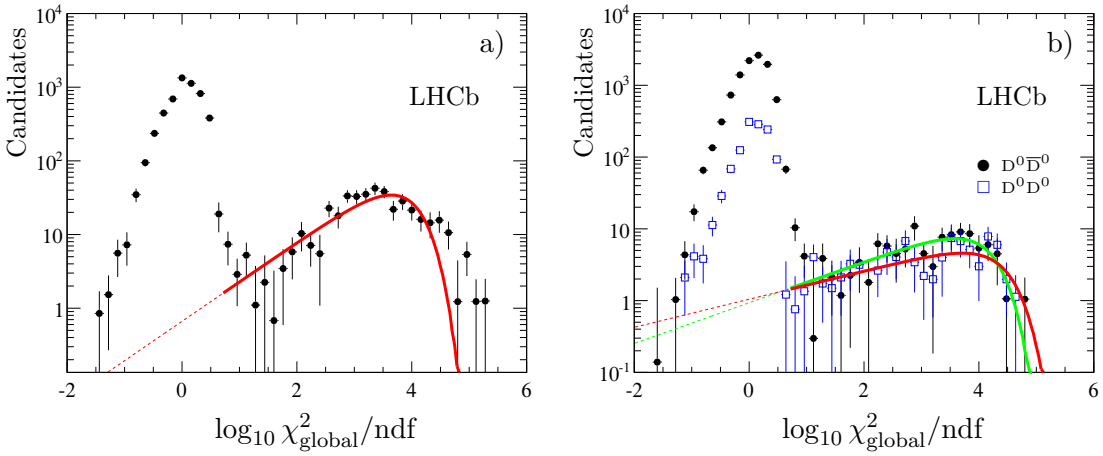

Figure 3. a) Background subtracted distribution of $\log_{10}\chi^2_{\rm global}/{\rm ndf}$ for $J/\psi\,D^0$ events. The solid line corresponds to the fit result in the region $\chi^2_{\rm global}/{\rm ndf} > 5$ by the function described in the text, the dashed line corresponds to the extrapolation of the fit results to the $\chi^2_{\rm global}/{\rm ndf} < 5$ region. b) Likewise for D^0D^0 (blue squares and red line) and $D^0\overline{D}{}^0$ (black circles and green line).

density functions (PDFs) for single open or hidden charm production described in section 3. These basic PDFs are used to build the components of the two dimensional mass fit. Let i and j denote the two resonance species. The reconstructed signal samples consist of the following components:

- Di-charm signal. This is modelled by a product PDF of the individual signal components for the first and the second particle.
- Combinatorial background. This is modelled by a product PDF of the individual background components i and j denoted by $B_i(m_i)$ and $B_j(m_j)$.
- Single production of component i together with combinatorial background for component j. This is modelled by a product PDF of the signal component i denoted $S_i(m_i)$ and the background component j denoted $B_j(m_j)$.
- Single production of component j together with combinatorial background for component i. This is modelled by a product PDF of the signal component j denoted $S_j(m_j)$ and the background component i denoted $B_i(m_i)$.

The total PDF is then

$$\begin{aligned} F(m_i, m_j) \propto & N^{S_i\times S_j} \times S_i(m_i)S_j(m_j) + N^{S_i\times B_j} \times S_i(m_i)B_j(m_j) \\ & + N^{B_i\times S_j} \times B_i(m_i)S_j(m_j) + N^{B_i\times B_j} \times B_{\rm i}(m_i)B_j(m_j), \end{aligned} \tag{4.1}$$

where $N^{S_i\times S_j}$, $N^{S_i\times B_j}$, $N^{B_i\times S_j}$ and $N^{B_i\times B_j}$ are the yields of the four components described above. The correctness of the fitting procedure is evaluated in simulation studies. As discussed in section 3 both the contribution of pile-up background and b-hadron decays is small and can be neglected. The goodness of fit is found to be acceptable using the distance to the nearest neighbour method described in refs. [28, 29].

JHEP06(2012)141

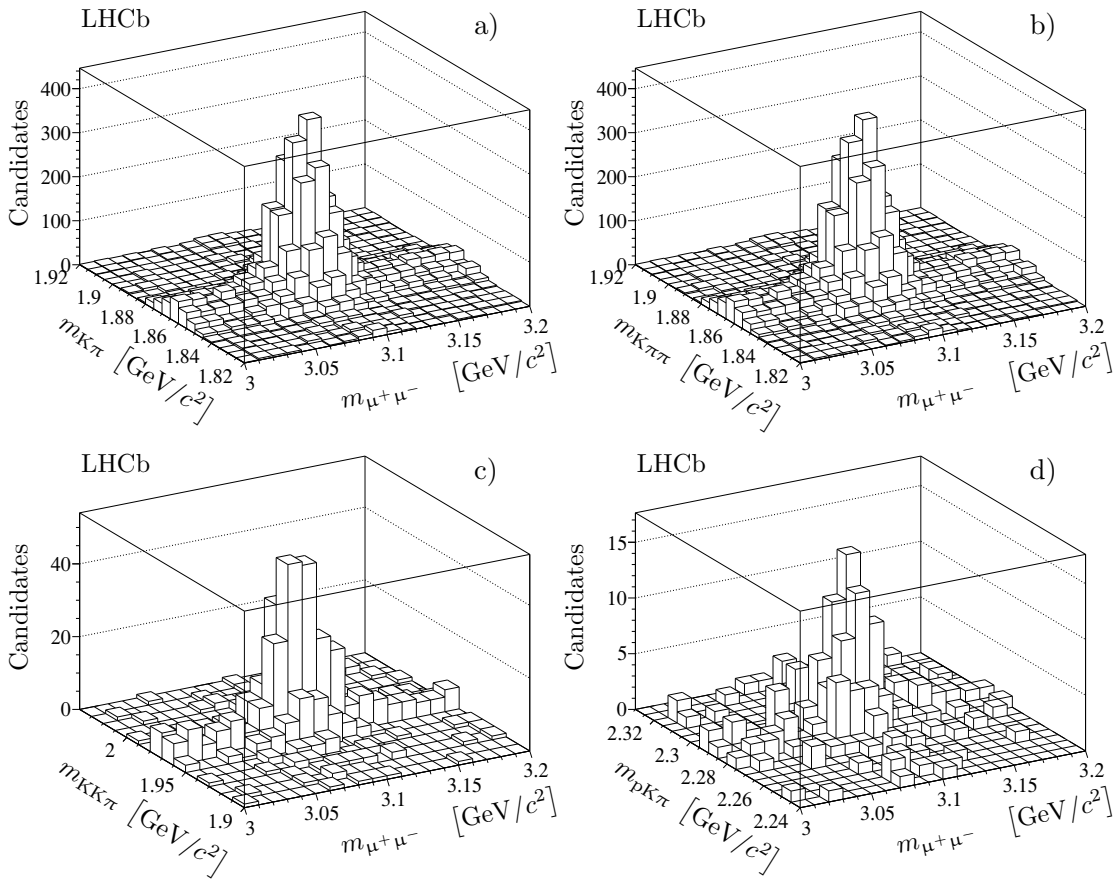

Figure 4. Invariant mass distributions for a) $J/\psi D^0$, b) $J/\psi D^+$, c) $J/\psi D_s^+$ and d) $J/\psi \Lambda_c^+$ candidates.

As a cross-check of the results, the signal yields have been determined from the single charm hadron mass spectra using the technique described in ref. [13]. In this approach, for each pair of charm species the invariant mass distributions of the first charm candidate are fitted to obtain the yield in bins of the invariant mass of the second candidate and vice versa. This technique gives signal yields consistent within 10% of the statistical uncertainty and also allows the statistical significance of the result to be easily evaluated. This exceeds five standard deviations for most of the modes considered. The signal yields for $J/\psi C$, CC and $C\overline{C}$ events are presented in tables 5 and 6 together with the estimate of the goodness of fit.

5 Efficiency correction

The yields are corrected for the detection efficiency to obtain the measured cross-sections. The efficiency for $J/\psi C$, $C\overline{C}$ and CC events $\varepsilon^{\rm tot}$ is computed for each signal event and is decomposed into three factors

$$\varepsilon^{\rm tot} = \varepsilon^{\rm reco} \times \varepsilon^{\rm ID} \times \varepsilon^{\rm trg}, \tag{5.1}$$

JHEP06(2012)141

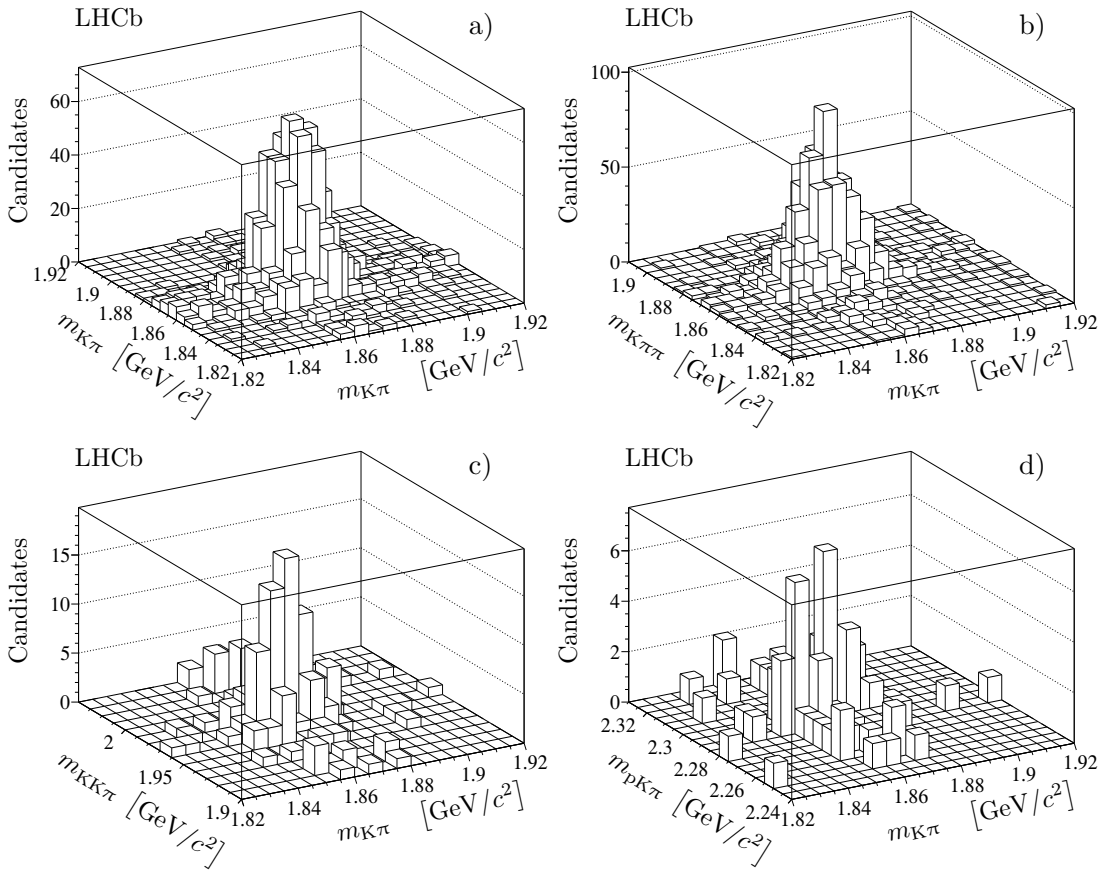

Figure 5. Invariant mass distributions for D^0C candidates: a) D^0D^0, b) D^0D^+, c) $D^0D_s^+$ and d) $D^0\Lambda_c^+$.

Mode	S	S_σ	P [%]
$J/\psi\,D^0$	4875 ± 86		59
$J/\psi\,D^+$	3323 ± 71		26
$J/\psi\,D_s^+$	328 ± 22		65
$J/\psi\,\Lambda_c^+$	116 ± 14	7.3σ	98

Table 5. Yields of $J/\psi\,C$ events, S, statistical significance of the signals, S_σ, determined from fits based on the technique described in ref. [13], and goodness-of-fit characteristic (χ^2 probability), P. When no significance is quoted, it is in excess of 8σ.

where $\varepsilon^{\rm reco}$ is the efficiency for acceptance, reconstruction and selection, $\varepsilon^{\rm ID}$ is the efficiency for particle identification and $\varepsilon^{\rm trg}$ is the trigger efficiency. The first term in eq. (5.1), $\varepsilon^{\rm reco}$ is factorized into the product of efficiencies for the first and second charm particle and a correction factor

$$\varepsilon^{\rm reco} = \varepsilon_1^{\rm reco} \times \varepsilon_2^{\rm reco} \times \xi^{\rm trk}, \tag{5.2}$$

JHEP06(2012)141

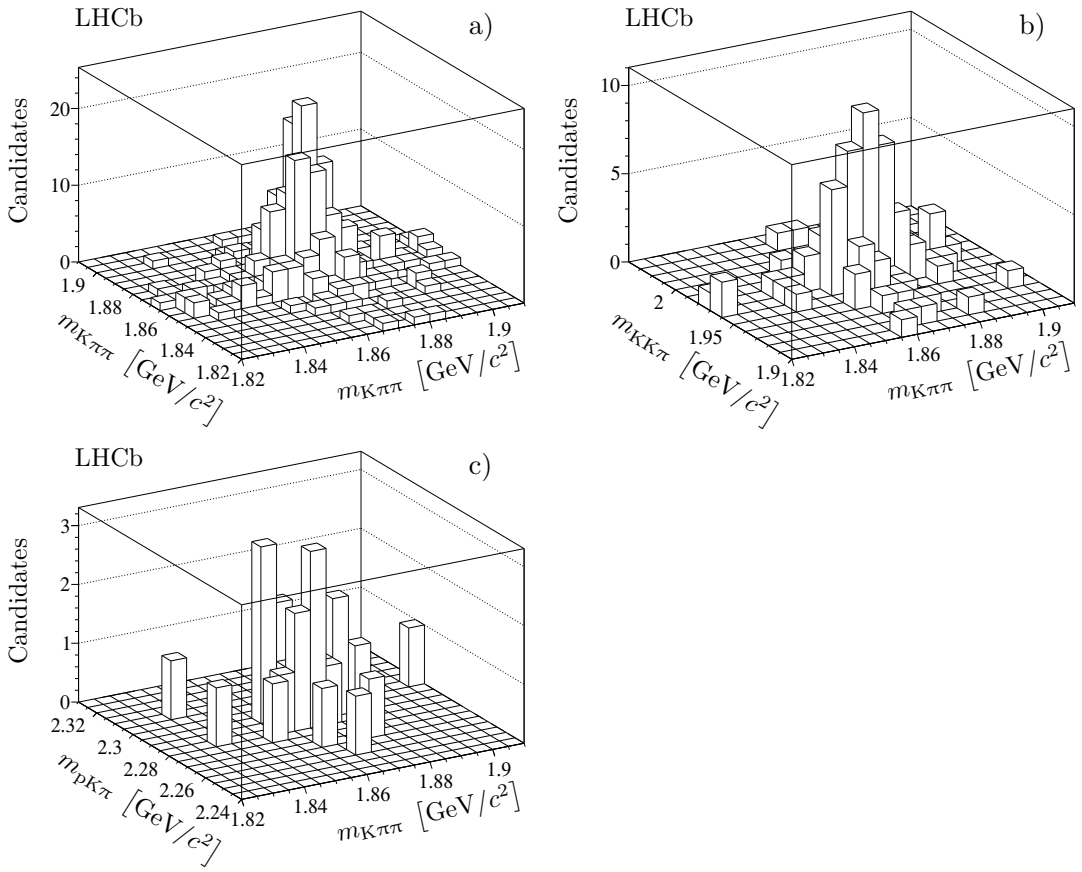

Figure 6. Invariant mass distributions for D^+C candidates: a) D^+D^+, b) $D^+D_s^+$, and c) $D^+\Lambda_c^+$.

where the efficiencies $\varepsilon^{\rm reco}_{(1,2)}$ are evaluated using the simulation, and the correction factor[3] $\xi^{\rm trk}$ is determined from the J/ψ data using a *tag-and-probe* method and accounts for relative differences in the track reconstruction efficiency between data and simulation.

The efficiency $\varepsilon_i^{\rm reco}$ is determined using the simulation in bins of rapidity y and transverse momentum $p^{\rm T}$ of the charm hadron. In the case of the J/ψ meson, the effect of the unknown polarization on the efficiency is accounted for by binning in $|\cos\theta^*_{\rm J/\psi}|$, where $\theta^*_{\rm J/\psi}$ is the angle between the μ^+ momentum in the J/ψ centre-of-mass frame and the J/ψ flight direction in the laboratory frame.

The efficiency for hadron identification as a function of momentum and pseudorapidity is determined from the data using samples of $D^{*+} \to \left(D^0 \to K^-\pi^+\right)\pi^+$, and $\Lambda \to p\pi^-$ [30, 31]. The efficiency for dimuon identification, $\varepsilon^{\rm ID}_{\rm J/\psi}$ is obtained from the analysis of the $J/\psi \to \mu^+\mu^-$ sample as a function of transverse momentum and rapidity of the J/ψ.

For the J/ψ C sample the J/ψ particle is required to trigger the event whilst for the CC and $C\overline{C}$ case either of the two charm mesons could trigger the event. The trigger efficiency for the di-charm system in the two cases is thus

$$\varepsilon^{\rm trg}_{\rm J/\psi\,C} = \varepsilon^{\rm trg}_{\rm J/\psi} \tag{5.3a}$$

$$\varepsilon^{\rm trg}_{C\overline{C},CC} = 1 - (1-\varepsilon^{\rm trg}_{C_1}) \times (1-\varepsilon^{\rm trg}_{C_2}). \tag{5.3b}$$

[3]This is the product of the individual corrections for each track.

JHEP06(2012)141

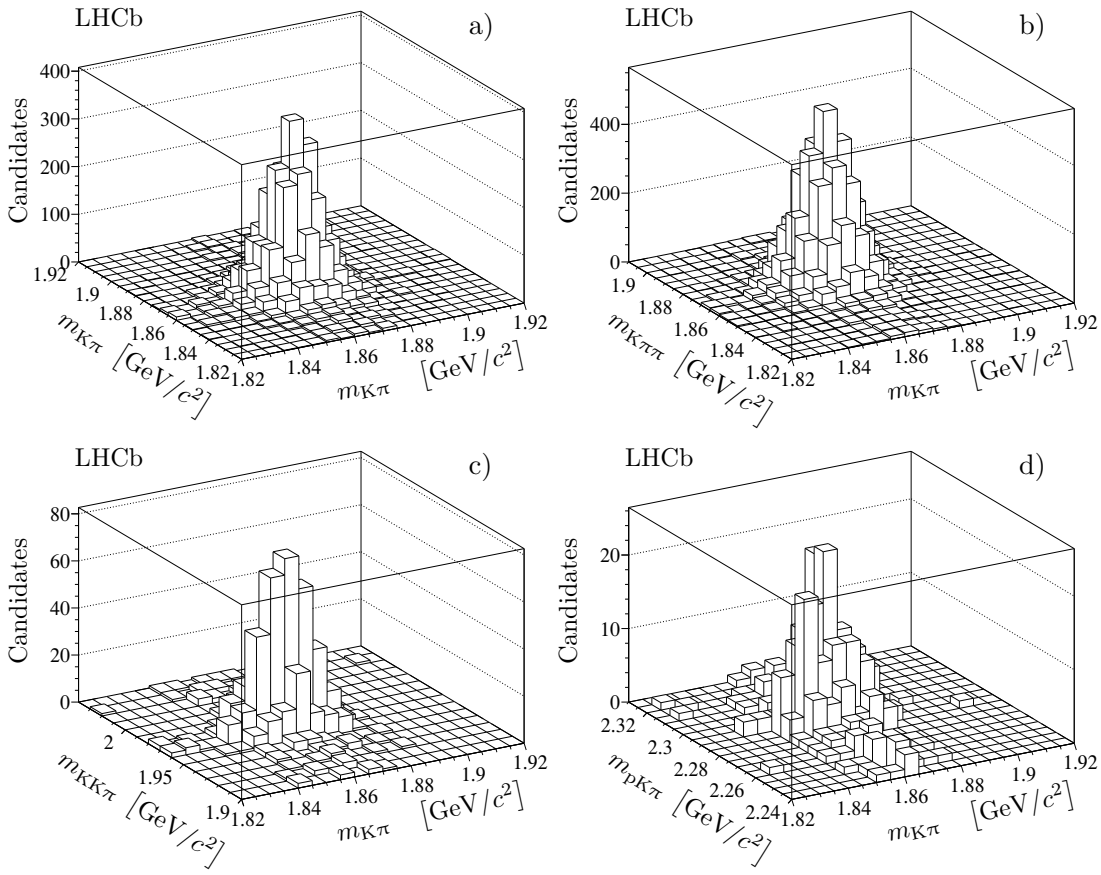

Figure 7. Invariant mass distributions for $D^0\bar{C}$ candidates: a) $D^0\overline{D}^0$, b) D^0D^-, c) $D^0D_s^-$ and d) $D^0\bar{\Lambda}_c^-$.

In both cases the trigger efficiency for a single charm hadron $\varepsilon^{\rm trg}_{\rm J/\psi}$ or $\varepsilon^{\rm trg}_{\rm C}$ is determined directly from the data using the inclusive prompt charm sample as a function of y and $p^{\rm T}$. This is done using a method that exploits the fact that events with prompt charm hadrons can be triggered either by the decay products of the charm hadron, or by the rest of the event [13, 32]. The overlap between the two cases allows the trigger efficiency to be estimated.

As discussed in section 2, global event cuts are applied in the trigger on the sub-detector hit multiplicites to reject complex events. The efficiency of these cuts $\varepsilon^{\rm GEC}$ is studied using the distributions of hit multiplicity after background subtraction. These distributions have been extrapolated from the regions unaffected by the cuts into the potentially affected regions and compared with the observed distributions in order to determine $\varepsilon^{\rm GEC}$.

The efficiency-corrected signal yield $N^{\rm corr}$ is determined using the ${}_s\mathcal{P}lot$ [33] technique. Each candidate is given a weight for it to be signal, ω_i, based on the result of the fit to the mass distributions described before. The weight is then divided by the total event efficiency and summed to give the efficiency-corrected yield

$$N^{\rm corr} = \sum_i \frac{\omega_i}{\varepsilon_i^{\rm tot}}. \tag{5.4}$$

JHEP06(2012)141

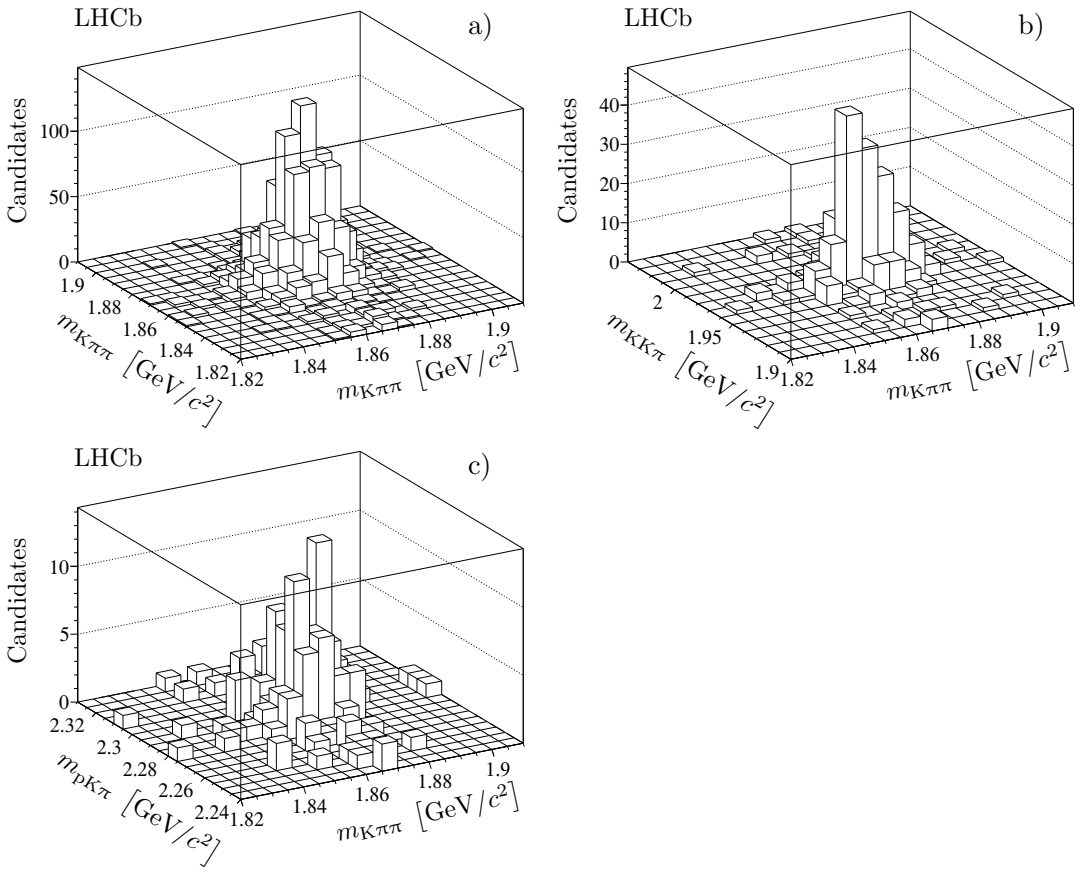

Figure 8. Invariant mass distributions for $C\overline{C}$ candidates: a) D^+D^-, b) $D^+D_s^-$ and c) $D^+\bar{\Lambda}_c^-$.

In the case of the D^0C and $D^0\overline{C}$ final states the corresponding yields have been corrected to take into account the double Cabibbo-suppressed decay (DCS) mode $D^0 \to K^+\pi^-$, which mixes the D^0C and $D^0\overline{C}$ reconstructed final states

$$\begin{pmatrix} N'_{D^0C} \\ N'_{D^0\bar{C}} \end{pmatrix} = \frac{1}{\sqrt{1-r^2}} \begin{pmatrix} 1 & -r \\ -r & 1 \end{pmatrix} \times \begin{pmatrix} N^{\rm corr}_{D^0C} \\ N^{\rm corr}_{D^0\bar{C}} \end{pmatrix}, \tag{5.5}$$

where r is $r^{\rm DCS} = \dfrac{\Gamma\left(D^0 \to K^+\pi^-\right)}{\Gamma\left(D^0 \to K^-\pi^+\right)} = (3.80 \pm 0.18)\times 10^{-3}$ [34]. This value of $r^{\rm DCS}$ accounts also for the effect of D^0-$\overline{D}^0$ mixing. For the D^0D^0 and $D^0\overline{D}^0$ cases the value of $r = 2r^{\rm DCS}$ is used.

6 Systematic uncertainties

The sources of systematic uncertainty that enter into the cross-section determination in addition to those related to the knowledge of branching ratios and luminosity are discussed below. The dominant source of systematic uncertainty arises from possible differences in the track reconstruction efficiency between data and simulation which are not accounted

JHEP06(2012)141

Mode	S	S_σ	P [%]
D^0D^0	1087 ± 37		4.5
$D^0\overline{D}^0$	10080 ± 105		33
D^0D^+	1177 ± 39		24
D^0D^-	11224 ± 112		36
$D^0D_s^+$	111 ± 12	8σ	10
$D^0D_s^-$	859 ± 31		13
$D^0\Lambda_c^+$	41 ± 8	5σ	9
$D^0\bar{\Lambda}_c^-$	308 ± 19		35
D^+D^+	249 ± 19		15
D^+D^-	3236 ± 61		67
$D^+D_s^+$	52 ± 9	5σ	54
$D^+D_s^-$	419 ± 22		59
$D^+\Lambda_c^+$	21 ± 5	2.5σ	36
$D^+\bar{\Lambda}_c^-$	137 ± 14	8σ	7

Table 6. Yields of CC and C$\overline{\text{C}}$ events, S, statistical significance of the signals, S_σ, determined from fits based on the technique, described in ref. [13], and goodness-of-fit characteristic, P. When no significance is quoted, it is in excess of 8σ.

for in the per-event efficiency. This includes the knowledge of the hadronic interaction length of the detector which results in an uncertainty of 2% per final state hadron [32]. An additional uncertainty is due to the statistical uncertainty on the determination of the per-event efficiency due to the finite size of the simulation and calibration samples. This is estimated by varying the obtained efficiencies within their corresponding uncertainties. The unknown polarization of J/ψ mesons affects the acceptance, reconstruction and selection efficiency $\varepsilon^{\text{reco}}_{\text{J/}\psi}$ [2]. In this analysis the effect is reduced by explicitly taking into account the dependence of $\varepsilon^{\text{reco}}_{\text{J/}\psi}$ on $|\cos\theta^*_{\text{J/}\psi}|$ in the efficiency determination. The remaining dependence results in a systematic uncertainty of 3% for channels containing a J/ψ.

Additional uncertainties are due to differences between data and simulation, uncertainty on the global event cuts, knowledge of the branching fractions of charm hadrons, $\mathcal{B}_i$. Uncertainties due to the parameterization of the signal and background components are found to be negligible.

The absolute luminosity scale was measured at specific periods during the data taking, using both van der Meer scans [35] where colliding beams are moved transversely across each other to determine the beam profile, and a beam-gas imaging method [36, 37]. For the latter, reconstructed beam-gas interaction vertices near the beam crossing point determine the beam profile. The knowledge of the absolute luminosity scale is used to calibrate the

JHEP06(2012)141

Source		$J/\psi D^0$	$J/\psi D^+$	$J/\psi D_s^+$	$J/\psi \Lambda_c^+$
J/ψ reconstruction	$\varepsilon_1^{\rm reco}$	1.3	1.3	1.3	1.3
C reconstruction	$\varepsilon_2^{\rm reco}$	0.7	0.8	1.7	3.3
Muon ID	$\varepsilon_{J/\psi}^{\rm ID}$	1.1	1.1	1.1	1.1
Hadron ID	$\varepsilon_{\rm had}^{\rm ID}$	1.1	1.9	1.1	1.5
Tracking	$\xi^{\rm trk}$	4.9	7.0	7.0	7.0
Trigger	$\varepsilon_{J/\psi C}^{\rm trg}$	3.0	3.0	3.0	3.0
J/ψ polarization	$\varepsilon_{J/\psi}^{\rm reco}$	3.0	3.0	3.0	3.0
Global event cuts	$\varepsilon^{\rm GEC}$	0.7	0.7	0.7	0.7
Luminosity	$\mathcal{L}$	3.7	3.7	3.7	3.7
$\mathcal{B}(J/\psi \to \mu^+\mu^-)$	$\mathcal{B}_1$	1.0	1.0	1.0	1.0
C branching fractions	$\mathcal{B}_2$	1.3	4.3	6.0	26
Total		8	10	11	28

Table 7. Relative systematic uncertainties (%) for the $J/\psi C$ cross-sections.

number of tracks in the silicon-strip vertex detector, which is found to be stable throughout the data-taking period and can therefore be used to monitor the instantaneous luminosity of the entire data sample. The dataset for this analysis corresponds to an integrated luminosity of 355 ± 13 pb^{-1}.

The sources of systematic uncertainty on the $J/\psi C$ production cross-section measurements are summarized in table 7 and those for open charm in tables 8 and 9. The total systematic uncertainties have been evaluated taking correlations into account where appropriate.

7 Results

The model-independent cross-section for double charm production in the fiducial range is computed as

$$\sigma = \frac{N^{\rm corr}}{\mathcal{L} \times \mathcal{B}_1 \times \mathcal{B}_2 \times \varepsilon^{\rm GEC}}, \tag{7.1}$$

where $\mathcal{L}$ is the integrated luminosity obtained as described in section 6, $\mathcal{B}_{(1,2)}$ stand for the corresponding branching ratios, $\varepsilon^{\rm GEC}$ is the efficiency of the global event cuts, and $N^{\rm corr}$ is the efficiency-corrected event yield, calculated according to eq. (5.4). The branching ratios used for these calculations are taken from ref. [34].

The cross-sections for the production of J/ψ and associated open charm, $\sigma_{J/\psi C}$, are measured in the fiducial volume $2 < y_{J/\psi}, y_C < 4$, $p_{J/\psi}^{\rm T} < 12$ GeV/c, $3 < p_C^{\rm T} < 12$ GeV/c. The results are summarized in table 10 and figure 9.

JHEP06(2012)141

Source		D^0D^0	D^0D^+	$D^0D_s^+$	$D^0\Lambda_c^+$
D^0C reconstruction	$\varepsilon_1^{\rm reco} \times \varepsilon_2^{\rm reco}$	1.4	1.4	2.3	3.6
Hadron ID	$\varepsilon_{\rm had}^{\rm ID}$	1.2	1.8	1.6	2.4
Tracking	$\xi^{\rm trk}$	8.5	10.7	10.6	10.6
Trigger	$\varepsilon_{\rm CC,C\overline{C}}^{\rm trg}$	1.8	2.5	3.9	5.2
Global event cuts	$\varepsilon^{\rm GEC}$	1.0	1.0	1.0	1.0
Luminosity	$\mathcal{L}$	3.7	3.7	3.7	3.7
$\mathcal{B}(D^0 \to K^-\pi^+)$	$\mathcal{B}_1$	1.3	1.3	1.3	1.3
C branching fractions	$\mathcal{B}_2$	1.3	4.3	6.0	26
Total		10	12	14	30

Table 8. Relative systematic uncertainties (%) for the D^0C cross-sections. The uncertainties for CC and $C\overline{C}$ are equal.

Source		D^+D^+	$D^+D_s^+$	$D^+\Lambda_c^+$
D^+C reconstruction	$\varepsilon_1^{\rm reco} \times \varepsilon_2^{\rm reco}$	1.4	2.2	4.0
Hadron ID	$\varepsilon_{\rm had}^{\rm ID}$	2.3	2.4	3.0
Tracking	$\xi^{\rm trk}$	12.8	12.8	12.8
Trigger	$\varepsilon_{\rm CC,C\overline{C}}^{\rm trg}$	3.7	5.8	5.0
Global event cuts	$\varepsilon^{\rm GEC}$	1.0	1.0	1.0
Luminosity	$\mathcal{L}$	3.7	3.7	3.7
$\mathcal{B}(D^+ \to K^-\pi^+\pi^+)$	$\mathcal{B}_1$	4.3	4.3	4.3
C branching fractions	$\mathcal{B}_2$	4.3	6.0	26
Total		17	17	31

Table 9. Relative systematic uncertainties (%) for the D^+C cross-sections. The uncertainties for the CC and $C\overline{C}$ are equal.

The systematic uncertainties related to the reconstruction and trigger are reduced if ratios to the cross-sections for prompt J/ψ, $\sigma_{J/\psi}$, and prompt open charm production, σ_C, with the same fiducial requirements are considered (taking into account correlated uncertainties) [1, 2]. These ratios are presented in table 11.

The cross-sections for CC and $C\overline{C}$ events in the fiducial volume $2 < y_C < 4$, $3 < p_C^T < 12$ GeV/c are measured and listed in table 12 and figure 9. The table also includes the ratio of CC and $C\overline{C}$ production cross-sections, $\sigma_{CC}/\sigma_{C\overline{C}}$, and the ratios of the product of the prompt open charm cross-sections to the CC ($C\overline{C}$) cross-sections, $\sigma_{C_1}\sigma_{C_2}/\sigma_{C_1C_2}$.

JHEP06(2012)141

Mode	σ [nb]
$J/\psi D^0$	$161.0 \pm 3.7 \pm 12.2$
$J/\psi D^+$	$56.6 \pm 1.7 \pm 5.9$
$J/\psi D_s^+$	$30.5 \pm 2.6 \pm 3.4$
$J/\psi \Lambda_c^+$	$43.2 \pm 7.0 \pm 12.0$

Table 10. Production cross-sections for $J/\psi C$. The first uncertainty is statistical, and the second is systematic.

Mode	$\sigma_{J/\psi C}/\sigma_{J/\psi}$ $[10^{-3}]$	$\sigma_{J/\psi C}/\sigma_C$ $[10^{-4}]$	$\sigma_{J/\psi}\sigma_C/\sigma_{J/\psi C}$ [mb]
$J/\psi D^0$	$16.2 \pm 0.4 \pm 1.3^{+3.4}_{-2.5}$	$6.7 \pm 0.2 \pm 0.5$	$14.9 \pm 0.4 \pm 1.1^{+2.3}_{-3.1}$
$J/\psi D^+$	$5.7 \pm 0.2 \pm 0.6^{+1.2}_{-0.9}$	$5.7 \pm 0.2 \pm 0.4$	$17.6 \pm 0.6 \pm 1.3^{+2.8}_{-3.7}$
$J/\psi D_s^+$	$3.1 \pm 0.3 \pm 0.4^{+0.6}_{-0.5}$	$7.8 \pm 0.8 \pm 0.6$	$12.8 \pm 1.3 \pm 1.1^{+2.0}_{-2.7}$
$J/\psi \Lambda_c^+$	$4.3 \pm 0.7 \pm 1.2^{+0.9}_{-0.7}$	$5.5 \pm 1.0 \pm 0.6$	$18.0 \pm 3.3 \pm 2.1^{+2.8}_{-3.8}$

Table 11. Ratios of $J/\psi C$ production cross-section to prompt J/ψ cross-section and prompt open charm cross-section, and ratios of the product of prompt J/ψ and open charm cross-sections to the $J/\psi C$ cross-section. The first uncertainty is statistical, the second is systematic, and the third is due to the unknown polarization of the prompt J/ψ [2].

Several of the estimations given in table 1 are also shown in figure 9 to compare with our measurements. The expectations from gluon-gluon fusion processes [14, 15, 18] are significantly below the measured cross-sections while the DPS estimates qualitatively agree with them. The observed ratio of $CC/C\overline{C}$ events is relatively large, e.g. compared with $\sigma_{J/\psi J/\psi}/\sigma_{J/\psi} = (5.1 \pm 1.0 \pm 1.1) \times 10^{-4}$ [13].

For the ratios $\sigma_{J/\psi}\sigma_C/\sigma_{J/\psi C}$ and $\sigma_{C_1}\sigma_{C_2}/\sigma_{C_1C_2}$ listed in tables 11 and 12, the systematic uncertainties largely cancel. In addition, theoretical inputs such as the choice of the strong coupling constant and the charm quark fragmentation fractions should cancel allowing a more reliable comparison between theory and data. For the $J/\psi C$ and CC cases these ratios have a clear interpretation in the DPS approach [4–6] as the effective cross-section of eq. (1.1) which should be the same for all modes. For the $C\overline{C}$ case, neglecting the contribution from $c\bar{c}c\bar{c}$ production, this ratio is related by a model-dependent kinematical factor to the total charm production cross-section and should be independent of the final state under consideration. The values for the effective DPS cross-section (the right-hand column in table 11, and figure 10) calculated from the $J/\psi C$ cross-section are in good agreement with the value measured in multi-jet production at the Tevatron $\sigma_{\text{eff}}^{\text{DPS}} = 14.5 \pm 1.7^{+1.7}_{-2.3}$ mb [16]. The effective cross-section extracted from the CC measurements is higher than this by a factor of typically two to three.

JHEP06(2012)141

Mode	σ [nb]	$\sigma_{CC}/\sigma_{C\overline{C}}$ [%]	$\sigma_{C_1}\sigma_{C_2}/\sigma_{C_1C_2}$ [mb]
D^0D^0	$690 \pm 40 \pm 70$	10.9 ± 0.8	$2 \times (42 \pm 3 \pm 4)$
$D^0\overline{D}^0$	$6230 \pm 120 \pm 630$		$2 \times (4.7 \pm 0.1 \pm 0.4)$
D^0D^+	$520 \pm 80 \pm 70$	12.8 ± 2.1	$47 \pm 7 \pm 4$
D^0D^-	$3990 \pm 90 \pm 500$		$6.0 \pm 0.2 \pm 0.5$
$D^0D_s^+$	$270 \pm 50 \pm 40$	15.7 ± 3.4	$36 \pm 8 \pm 4$
$D^0D_s^-$	$1680 \pm 110 \pm 240$		$5.6 \pm 0.5 \pm 0.6$
$D^0\bar{\Lambda}_c^-$	$2010 \pm 280 \pm 600$	—	$9 \pm 2 \pm 1$
D^+D^+	$80 \pm 10 \pm 10$	9.6 ± 1.6	$2 \times (66 \pm 11 \pm 7)$
D^+D^-	$780 \pm 40 \pm 130$		$2 \times (6.4 \pm 0.4 \pm 0.7)$
$D^+D_s^+$	$70 \pm 15 \pm 10$	12.1 ± 3.3	$59 \pm 15 \pm 6$
$D^+D_s^-$	$550 \pm 60 \pm 90$		$7 \pm 1 \pm 1$
$D^+\Lambda_c^+$	$60 \pm 30 \pm 20$	10.7 ± 5.9	$140 \pm 70 \pm 20$
$D^+\bar{\Lambda}_c^-$	$530 \pm 130 \pm 170$		$15 \pm 4 \pm 2$

Table 12. Production cross-sections for CC and $C\overline{C}$, ratios of the CC and $C\overline{C}$ cross-sections and ratios of the product of prompt open charm cross-sections to the CC ($C\overline{C}$) cross-sections. The first uncertainty is statistical and the second is systematic. The symmetry factor 2 is explicitly indicated for the D^0D^0, $D^0\overline{D}^0$, D^+D^+ and D^+D^- ratios.

JHEP06(2012)141

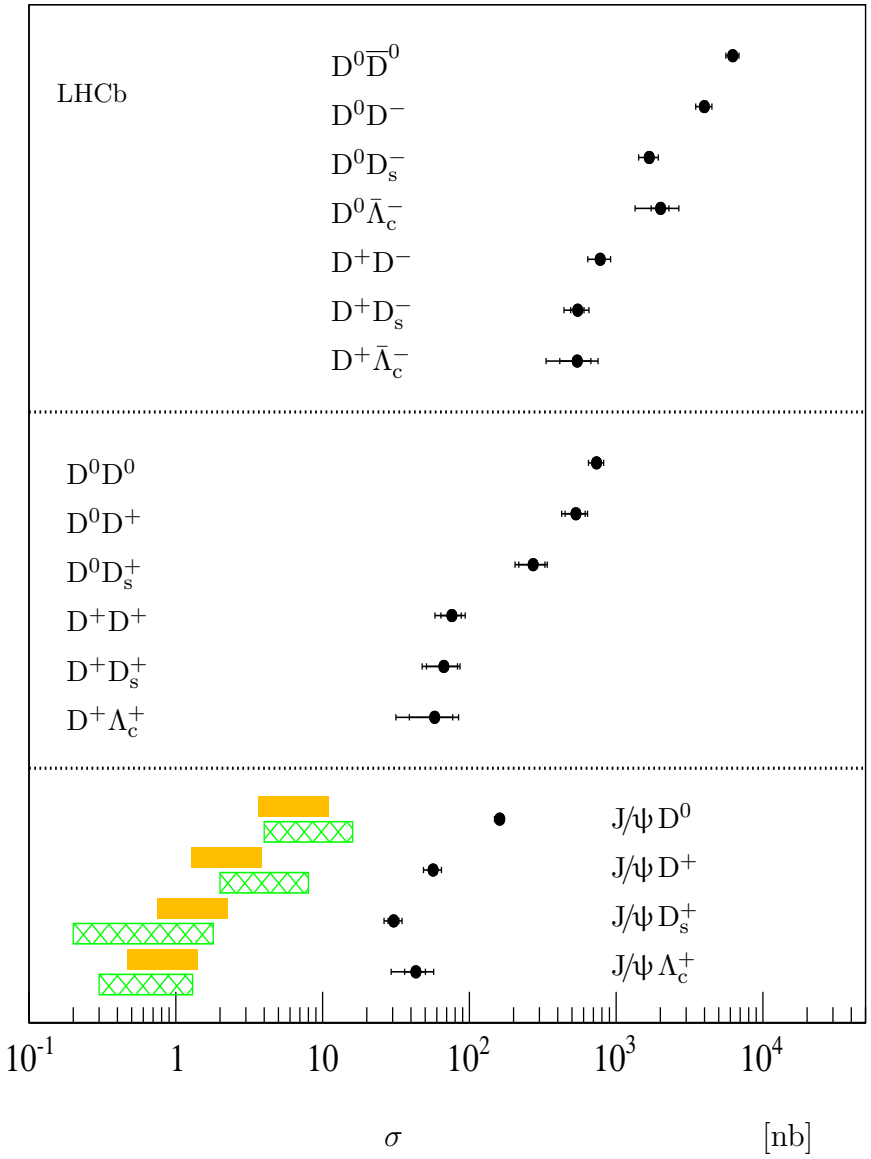

Figure 9. Measured cross-sections $\sigma_{J/\psi C}$, σ_{CC} and $\sigma_{C\overline{C}}$ (points with error bars) compared, in $J/\psi C$ channels, to the calculations in refs. [14, 15] (hatched areas) and ref. [18] (shaded areas). The inner error bars indicate the statistical uncertainty whilst the outer error bars indicate the sum of the statistical and systematic uncertainties in quadrature. Charge-conjugate modes are included.

JHEP06(2012)141

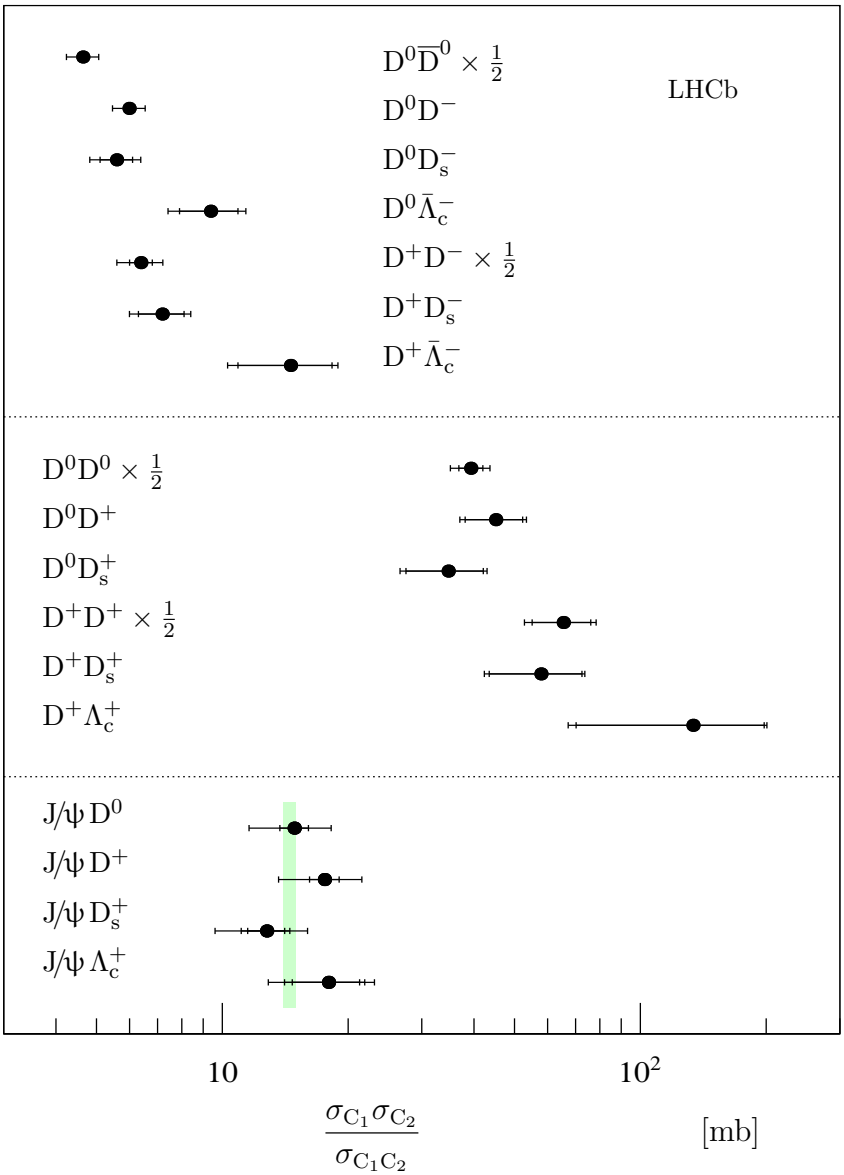

Figure 10. Measured ratios $\sigma_{C_1}\sigma_{C_2}/\sigma_{C_1C_2}$ (points with error bars) in comparison with the expectations from DPS using the cross-section measured at Tevatron for multi-jet events (light green shaded area). For the D^0D^0, $D^0\overline{D}{}^0$, D^+D^+ and D^+D^- cases the ratios are rescaled with the symmetry factor of one half. The inner error bars indicate the statistical uncertainty whilst the outer error bars indicate the sum of the statistical and systematic uncertainties in quadrature. For the $J/\psi\, C$ case the outermost error bars correspond to the total uncertainties including the uncertainties due to the unknown polarization of the prompt J/ψ mesons. Charge-conjugate modes are included.

JHEP06(2012)141

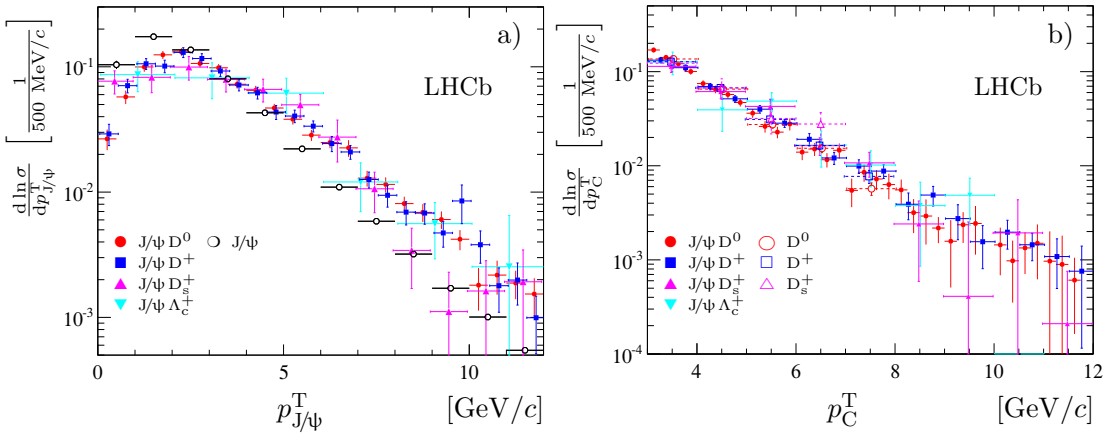

Figure 11. a) Transverse momentum spectra of J/ψ for J/ψ C and prompt J/ψ events. b) Transverse momentum spectra for open charm hadrons for J/ψ C and prompt D^0, D^+ and D_s^+ events.

8 Properties of J/ψ C, CC, and C$\overline{\text{C}}$ events

The data samples available also allow the properties of the multiple charm events to be studied. The transverse momentum spectra for J/ψ and open charm mesons in J/ψ C events are presented in figure 11.

The transverse momentum spectra of the J/ψ meson in J/ψ C events are similar for all species of open charm hadrons. The shape of the transverse momentum spectra of open charm hadrons also appears to be the same for all species. The $p^{\mathrm{T}}_{\mathrm{J/\psi}}$ spectra are harder than the corresponding spectrum of prompt J/ψ, while the p^{T}-spectra for open charm hadrons seem to be well compatible in shape with the spectra for prompt charm production. To allow a more quantitative comparison, each spectrum is fitted in the region $3 < p^{\mathrm{T}} < 12$ GeV/c with an exponential function. The results are summarized in table 13 and figure 14. They agree reasonably well within the uncertainties. The transverse momentum spectra of charm hadrons from CC and C$\overline{\text{C}}$ events are presented in figures 12 and 13. The fitted slope parameters of an exponential function are summarized in table 14 and figure 14. The p^{T}-slopes, though similar for C$\overline{\text{C}}$ and CC events, are significantly different from those for both single prompt charm particles and those found in J/ψ C events.

The correlations in azimuthal angle and rapidity between the two charm hadrons have also been studied by measuring the distributions of $\Delta\phi$ and Δy, where $\Delta\phi$ and Δy are the differences in azimuthal angle and rapidity between the two hadrons. These distributions for the charm hadrons in J/ψ C events are shown in figure 15. No significant azimuthal correlation is observed. The Δy distribution is compared to the triangular shape that is expected if the rapidity distribution for single charm hadrons is flat and if there are no correlations.

The azimuthal and rapidity correlations for CC and C$\overline{\text{C}}$ events are shown in figures 16, 17, and 18. In the CC case the $\Delta\phi$ distribution is reasonably consistent with a flat distribution. In contrast, for C$\overline{\text{C}}$ events a clear enhancement is seen for $\Delta\phi$ distributions at small $|\Delta\phi|$. This is consistent with c$\bar{\text{c}}$ production via the gluon splitting mechanism [38].

JHEP06(2012)141

Mode	p^{T}-slope $\left[\frac{1}{\mathrm{GeV}/c}\right]$	
	J/ψ	C
$\mathrm{J/\psi\,D^0}$	-0.49 ± 0.01	-0.75 ± 0.02
$\mathrm{J/\psi\,D^+}$	-0.49 ± 0.02	-0.65 ± 0.02
$\mathrm{J/\psi\,D_s^+}$	-0.60 ± 0.05	-0.68 ± 0.05
$\mathrm{J/\psi\,\Lambda_c^+}$	-0.46 ± 0.08	-0.82 ± 0.08
J/ψ	-0.633 ± 0.003	
$\mathrm{D^0}$		-0.77 ± 0.03
$\mathrm{D^+}$		-0.70 ± 0.03
$\mathrm{D_s^+}$		-0.57 ± 0.13
Λ_c^+		-0.79 ± 0.08

Table 13. Slope parameters of the transverse momentum spectra in the J/ψ C mode and for prompt charm particles. These parameters are determined from fits to the spectra in the region $3 < p^{\mathrm{T}} < 12$ GeV/c.

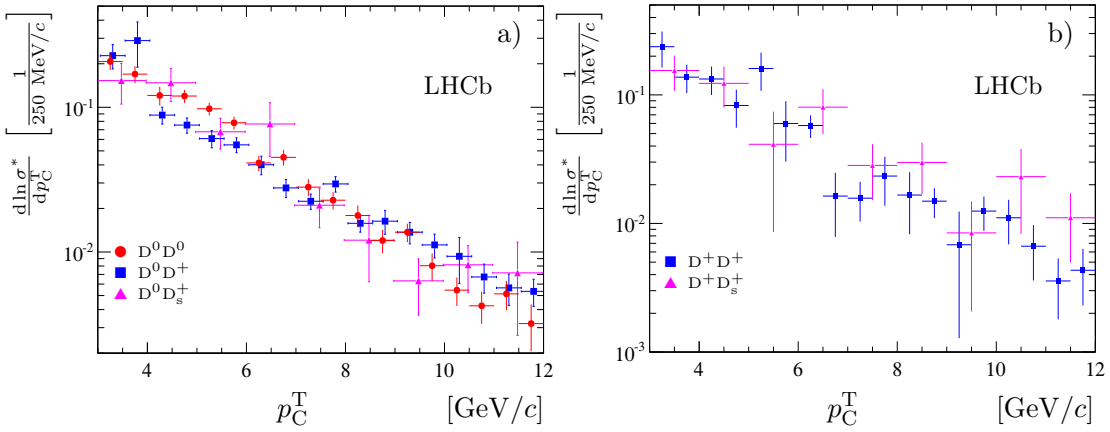

Figure 12. Transverse momentum spectra of charm hadrons from CC: a) $\mathrm{D^0D^0}$, $\mathrm{D^0D^+}$, $\mathrm{D^0D_s^+}$ and b) $\mathrm{D^+D^+}$ and $\mathrm{D^+D_s^+}$.

The $\mathrm{C\overline{C}}$ events suggest some enhancement at small $|\Delta y|$, while the CC sample shows no clear difference from the triangular shape given the present statistics.

Finally, the invariant mass distributions of the pairs of charm hadrons in these events have been studied. The mass spectra for J/ψ C and CC events are shown in figure 19. The spectra appear to be independent of the type of the open charm hadron.

The invariant mass spectra for $\mathrm{C\overline{C}}$ events are shown in figure 20. Again, the spectra are similar and independent of the type of the open charm meson. The enhancement at small invariant mass is most likely due to the gluon splitting process [38]. For the region of invariant masses above 6 GeV/c^2 the spectra are similar for $\mathrm{C\overline{C}}$ and CC events.

JHEP06(2012)141

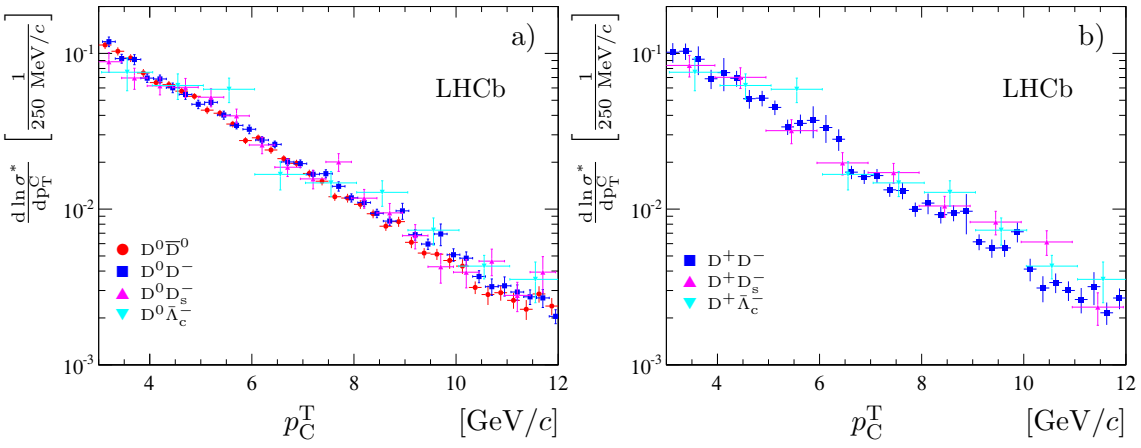

Figure 13. Transverse momentum spectra of charm hadrons from $\mathrm{C\overline{C}}$: a) $\mathrm{D^0\overline{D}^0}$, $\mathrm{D^0D^-}$, $\mathrm{D^0D_s^-}$ and $\mathrm{D^0\bar{\Lambda}_c^-}$; b) $\mathrm{D^+D^-}$, $\mathrm{D^+D_s^-}$ and $\mathrm{D^+\bar{\Lambda}_c^-}$.

Mode	p^{T}-slope $\left[\frac{1}{\mathrm{GeV}/c}\right]$
$\mathrm{D^0D^0}$	-0.51 ± 0.02
$\mathrm{D^0\overline{D}^0}$	-0.48 ± 0.01
$\mathrm{D^0D^+}$	-0.40 ± 0.02
$\mathrm{D^0D^-}$	-0.46 ± 0.01
$\mathrm{D^0D_s^+}$	-0.51 ± 0.05
$\mathrm{D^0D_s^-}$	-0.44 ± 0.02
$\mathrm{D^0\bar{\Lambda}_c^-}$	-0.41 ± 0.03
$\mathrm{D^+D^+}$	-0.48 ± 0.04
$\mathrm{D^+D^-}$	-0.46 ± 0.01
$\mathrm{D^+D_s^+}$	-0.39 ± 0.07
$\mathrm{D^+D_s^-}$	-0.42 ± 0.02
$\mathrm{D^+\bar{\Lambda}_c^-}$	-0.38 ± 0.05

Table 14. Slope parameters of transverse momentum spectra for the CC and $\mathrm{C\overline{C}}$ modes.

JHEP06(2012)141

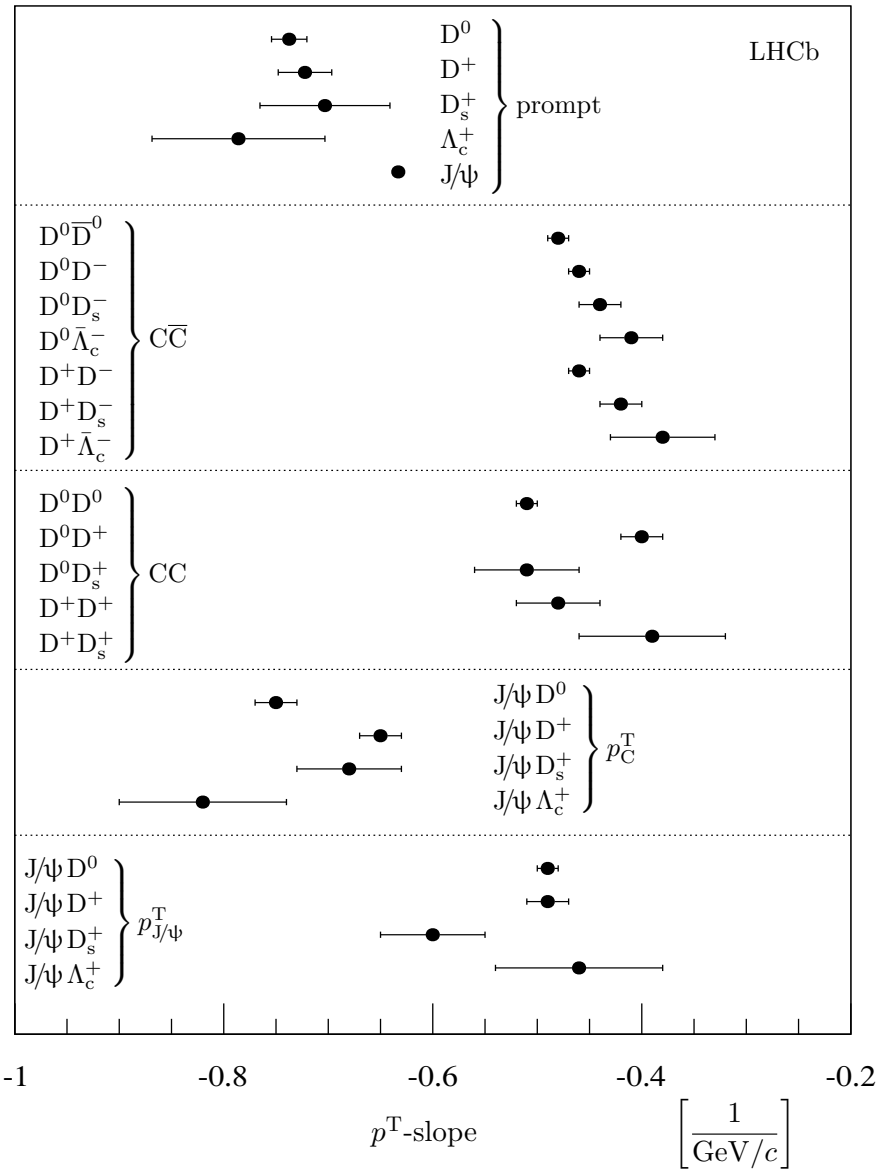

Figure 14. Slope parameters of the transverse momentum spectra for prompt charm particles [1] and charm particles from J/ψ C, $C\overline{C}$ and CC production.

JHEP06(2012)141

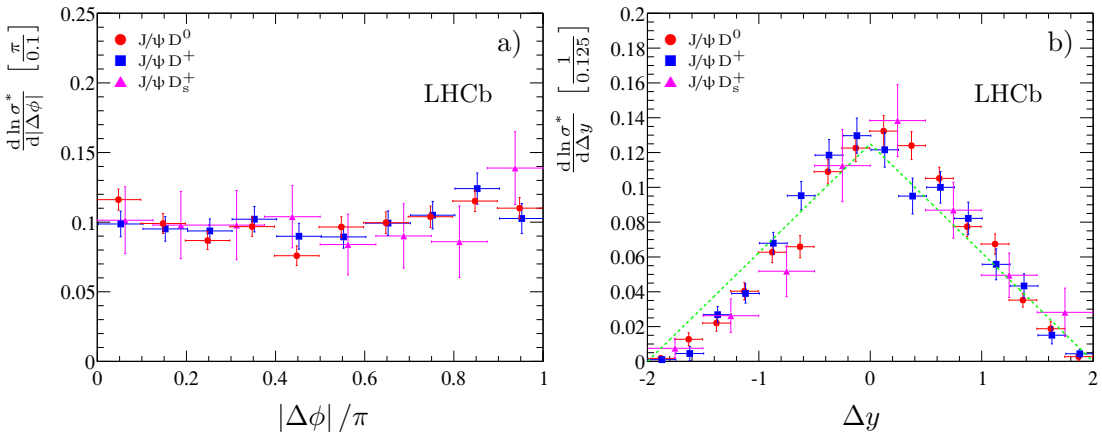

Figure 15. Distributions of the difference in azimuthal angle (a) and rapidity (b) for $J/\psi D^0$, $J/\psi D^+$ and $J/\psi D_s^+$ events. The dashed line shows the expected distribution for uncorrelated events.

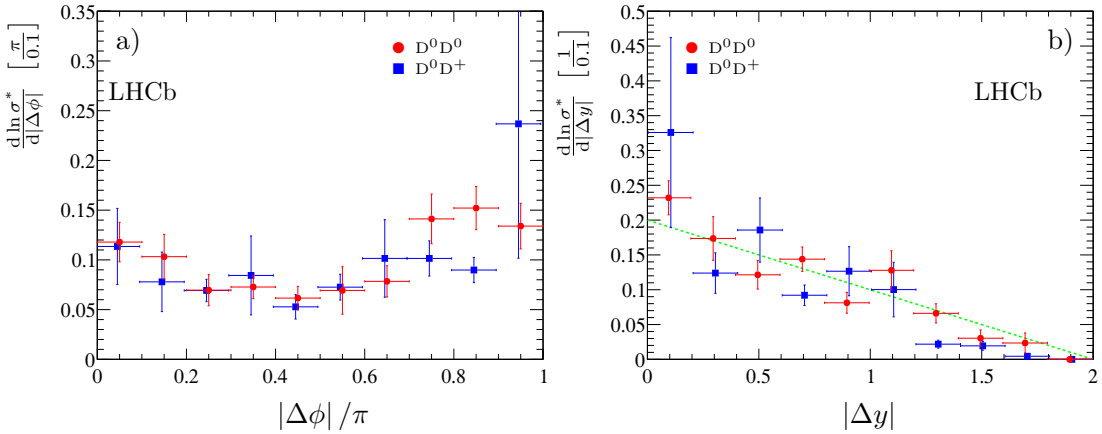

Figure 16. Distributions of the difference in azimuthal angle (a) and rapidity (b) for D^0D^0 and D^0D^+ events. The dashed line shows the expected distribution for uncorrelated events.

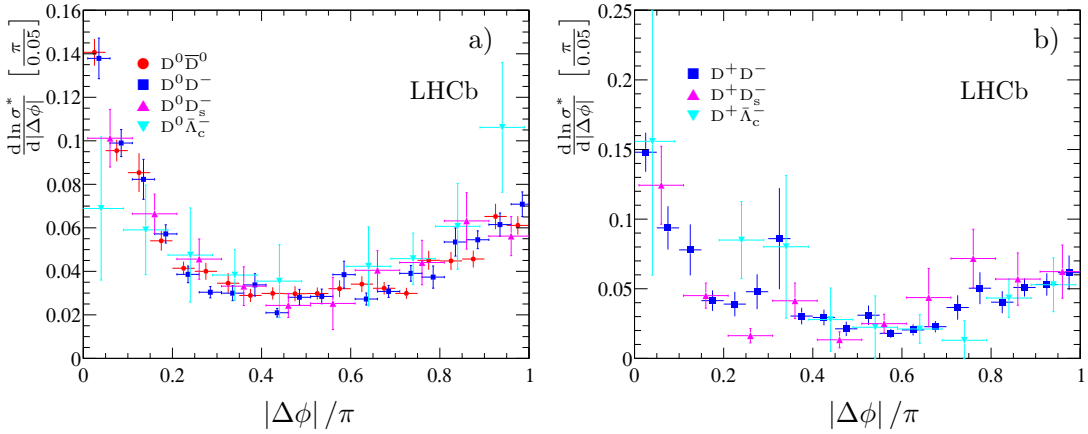

Figure 17. Distributions of the difference in azimuthal angle for $C\overline{C}$ events: a) $D^0\overline{D}^0$, D^0D^-, $D^0D_s^-$ and $D^0\bar{\Lambda}_c^-$; b) D^+D^-, $D^+D_s^-$ and $D^+\bar{\Lambda}_c^-$.

JHEP06(2012)141

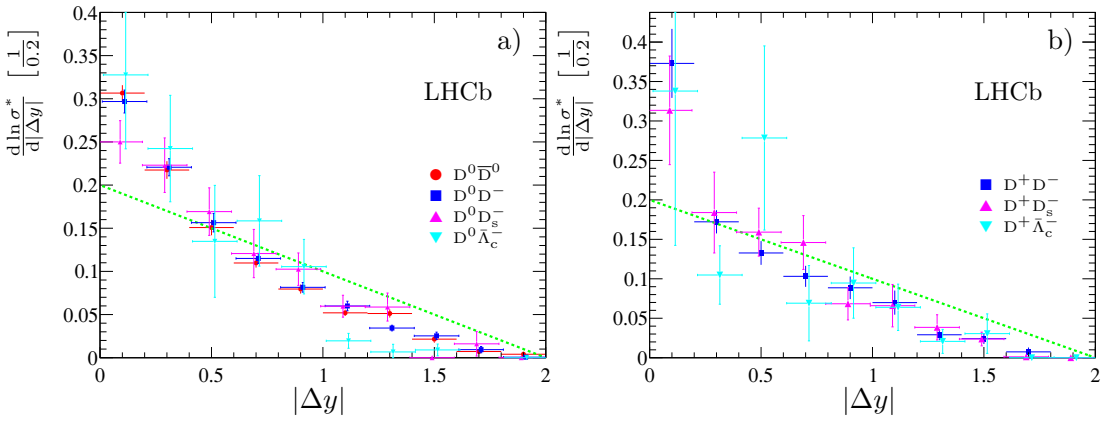

Figure 18. Distributions of the difference in rapidity for $C\overline{C}$ events: a) $D^0\overline{D}{}^0$, D^0D^-, $D^0D_s^-$ and $D^0\bar{\Lambda}_c^-$; b) D^+D^-, $D^+D_s^-$ and $D^+\bar{\Lambda}_c^-$. The dashed line shows the expected distribution for uncorrelated events.

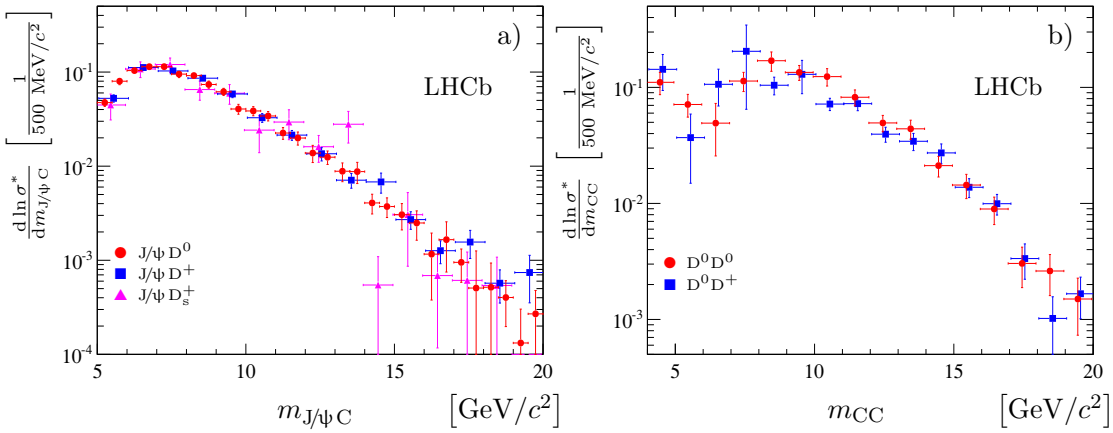

Figure 19. a) Invariant mass spectra for $J/\psi D^0$, $J/\psi D^+$ and $J/\psi D_s^+$ events. b) Invariant mass spectra for D^0D^0 and D^0D^+ events.

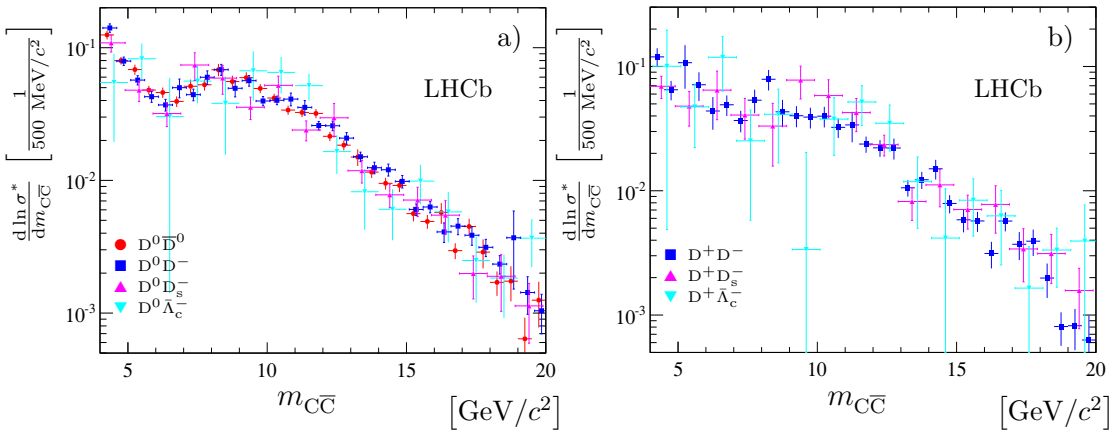

Figure 20. Invariant mass spectra for $C\overline{C}$ events: a) $D^0\overline{D}{}^0$, D^0D^-, $D^0D_s^-$ and $D^0\bar{\Lambda}_c^-$; b) D^+D^-, $D^+D_s^-$ and $D^+\bar{\Lambda}_c^-$.

JHEP06(2012)141

9 Conclusion

The production of J/ψ mesons accompanied by open charm, and pairs of open charm hadrons has been observed in pp collisions at $\sqrt{s} = 7$ TeV. This is the first observation of these phenomena in hadronic collisions. Signals with a statistical significance in excess of five standard deviations have been observed for four J/ψ C modes: $J/\psi\, D^0$, $J/\psi\, D^+$, $J/\psi\, D_s^+$ and $J/\psi\, \Lambda_c^+$, for six CC modes: D^0D^0, D^0D^+, $D^0D_s^+$, $D^0\Lambda_c^+$, D^+D^+, and $D^+D_s^+$, and for seven $C\overline{C}$ channels: $D^0\overline{D}^0$, D^0D^-, $D^0D_s^-$, $D^0\bar{\Lambda}_c^-$, D^+D^-, $D^+D_s^-$ and $D^+\bar{\Lambda}_c^-$.

The cross-sections and the properties of these events have been studied. The predictions from gluon-gluon fusion [14, 15, 18] are significantly smaller than the observed cross-sections. Better agreement is found with the DPS model [4–7] if the effective cross-section inferred from the Tevatron data is used. The absence of significant azimuthal or rapidity correlations provides support for this hypothesis. This interpretation is only partially supported by the CC data: if DPS is assumed to dominate, the estimated effective cross-section would be a factor 2-3 larger than in the J/ψ C case.

The transverse momentum spectra for these events have also been studied. The transverse momentum spectra for J/ψ from J/ψ C events are significantly harder than those observed in prompt J/ψ production. On the other hand the spectra for open charm mesons in J/ψ C events appear to be similar to those observed for prompt charm hadrons. Similar transverse momentum spectra for CC and $C\overline{C}$ events are observed. However, the expectation of similar transverse momentum spectra for $C\overline{C}$ events and prompt charm events appears to be invalid.

For $C\overline{C}$ events significant rapidity and azimuthal correlations are observed. These, as well as the invariant mass spectra for $C\overline{C}$ events, suggest a sizeable contribution from the gluon splitting process to charm quark production [38].

Acknowledgements

We would like to thank J.-P. Lansberg, A.K. Likhoded and A. Szczurek for many fruitful discussions. We express our gratitude to our colleagues in the CERN accelerator departments for the excellent performance of the LHC. We thank the technical and administrative staff at CERN and at the LHCb institutes, and acknowledge support from the National Agencies: CAPES, CNPq, FAPERJ and FINEP (Brazil); CERN; NSFC (China); CNRS/IN2P3 (France); BMBF, DFG, HGF and MPG (Germany); SFI (Ireland); INFN (Italy); FOM and NWO (The Netherlands); SCSR (Poland); ANCS (Romania); MinES of Russia and Rosatom (Russia); MICINN, XuntaGal and GENCAT (Spain); SNSF and SER (Switzerland); NAS Ukraine (Ukraine); STFC (United Kingdom); NSF (USA). We also acknowledge the support received from the ERC under FP7 and the Region Auvergne.

A Contribution from sea charm quarks

Estimates for the expected cross-section in the LHCb fiducial region due to the sea charm quarks from the interacting protons have been made as follows. The LHCb rapidity window

JHEP06(2012)141

$2 < y < 4$ corresponds to a x range for the additional charm quarks of

$$\frac{2m_{\mathrm{c}}^{\mathrm{T}}}{\sqrt{s}} \sinh 2 < x < \frac{2m_{\mathrm{c}}^{\mathrm{T}}}{\sqrt{s}} \sinh 4 \tag{A.1}$$

where $m_{\mathrm{c}}^{\mathrm{T}}$ is the transverse mass of the charm quark. Assuming the extra charm mesons are distributed over p^{T} in a similar way to the inclusive charm mesons measured in [1, 2] one can take

$$m_{\mathrm{c}}^{\mathrm{T}} \approx m_{\mathrm{c}} \oplus 2 \text{ GeV}/c^2, \tag{A.2}$$

where 2 GeV/c is the mean transverse momentum of charm quarks produced. This leads to the x range of $0.0026 < x < 0.02$. Integration of Alekhin's LO parton distribution functions [39] over this x range gives 0.25 additional charm quarks per event. In this calculation the parton density functions are taken at the scale $\mu \approx m_{\mathrm{J/\psi}}^{\mathrm{T}}$. The cross-sections of J/ψ plus open charm mesons can then be estimated using the probabilities for the c-quark transition to different mesons given in [1, 2]. Similarly cross-sections for double open charm production can be estimated. Taking $\mu \approx m_{\mathrm{D}}^{\mathrm{T}}$ and integrating Alekhin's LO parton density functions [39] on gets approximately 0.17 additional charm quarks per event. This calculation assumes that all extra charm quarks from protons hadronize to open charm states visible in the detector. The real cross-sections may be smaller, but the ratio of different open charm states is expected to remain the same. The integrated parton density functions provide no information about the p^{T} distribution of charm quarks. Under the assumption that the p^{T}-spectrum coincides with the distribution of prompt charm particles measured at LHCb [1], the cross-sections in the LHCb fiducial range are calculated (see last column of table 1).

References

[1] LHCb collaboration, *Prompt charm production in pp collisions at* $\sqrt{s} = 7$ *TeV*, LHCb-CONF-2010-013 (2010).

[2] LHCb collaboration, R. Aaij et al., *Measurement of* J/ψ *production in pp collisions at* $\sqrt{s} = 7$ *TeV*, *Eur. Phys. J.* **C 71** (2011) 1645 [arXiv:1103.0423] [INSPIRE].

[3] S.J. Brodsky and J.-P. Lansberg, *Heavy-quarkonium production in high energy proton-proton collisions at RHIC*, *Phys. Rev.* **D 81** (2010) 051502 [arXiv:0908.0754] [INSPIRE].

[4] C. Kom, A. Kulesza and W. Stirling, *Pair production of* J/ψ *as a probe of double parton scattering at LHCb*, *Phys. Rev. Lett.* **107** (2011) 082002 [arXiv:1105.4186] [INSPIRE].

[5] S. Baranov, A. Snigirev and N. Zotov, *Double heavy meson production through double parton scattering in hadronic collisions*, *Phys. Lett.* **B 705** (2011) 116 [arXiv:1105.6276] [INSPIRE].

[6] A. Novoselov, *Double parton scattering as a source of quarkonia pairs in LHCb*, arXiv:1106.2184 [INSPIRE].

JHEP06(2012)141

[7] M. Luszczak, R. Maciula and A. Szczurek, *Production of two $c\bar{c}$ pairs in double-parton scattering*, arXiv:1111.3255 [INSPIRE].

[8] S. Brodsky, P. Hoyer, C. Peterson and N. Sakai, *The intrinsic charm of the proton*, *Phys. Lett.* **B 93** (1980) 451 [INSPIRE].

[9] S. Aoki et al., *The double associated production of charmed particles by the interaction of 350 GeV/c π^- mesons with emulsion nuclei*, *Phys. Lett.* **B 187** (1987) 185 [INSPIRE].

[10] V. Kartvelishvili and S. Esakiya, *On hadron induced production of J/ψ meson pairs* (in Russian), *Yad. Fiz.* **38** (1983) 722 [INSPIRE].

[11] B. Humpert and P. Mery, *$\psi\psi$ production at collider energies*, *Z. Phys.* **C 20** (1983) 83 [INSPIRE].

[12] A. Berezhnoy, A. Likhoded, A. Luchinsky and A. Novoselov, *Double J/ψ-meson production at LHC and 4c-tetraquark state*, *Phys. Rev.* **D 84** (2011) 094023 [arXiv:1101.5881] [INSPIRE].

[13] LHCb collaboration, R. Aaij et al., *Observation of J/ψ pair production in pp collisions at $\sqrt{s} = 7$ TeV*, *Phys. Lett.* **B 707** (2012) 52 [arXiv:1109.0963] [INSPIRE].

[14] A. Berezhnoy, V. Kiselev, A. Likhoded and A. Onishchenko, *Doubly charmed baryon production in hadronic experiments*, *Phys. Rev.* **D 57** (1998) 4385 [hep-ph/9710339] [INSPIRE].

[15] S. Baranov, *Topics in associated $J/\psi + c + \bar{c}$ production at modern colliders*, *Phys. Rev.* **D 73** (2006) 074021 [INSPIRE].

[16] CDF collaboration, F. Abe et al., *Double parton scattering in $\bar{p}p$ collisions at $\sqrt{s} = 1.8$ TeV*, *Phys. Rev.* **D 56** (1997) 3811 [INSPIRE].

[17] B. Blok, Y. Dokshitser, L. Frankfurt and M. Strikman, *pQCD physics of multiparton interactions*, *Eur. Phys. J.* **C 72** (2012) 1963 [arXiv:1106.5533] [INSPIRE].

[18] J. Lansberg, *On the mechanisms of heavy-quarkonium hadroproduction*, *Eur. Phys. J.* **C 61** (2009) 693 [arXiv:0811.4005] [INSPIRE].

[19] LHCb collaboration, J. Alves, A. Augusto et al., *The LHCb detector at the LHC*, 2008 *JINST* **3** S08005 [INSPIRE].

[20] V. Gligorov, C. Thomas and M. Williams, *The HLT inclusive B triggers*, LHCb-PUB-2011-016 (2011).

[21] T. Sjöstrand, S. Mrenna and P.Z. Skands, *PYTHIA 6.4 physics and manual*, *JHEP* **05** (2006) 026 [hep-ph/0603175] [INSPIRE].

[22] I. Belyaev et al., *Handling of the generation of primary events in GAUSS, the LHCb simulation framework*, *Nucl. Sci. Symp. Conf. Rec.* (2010) 1155.

[23] D. Lange, *The EvtGen particle decay simulation package*, *Nucl. Instrum. Meth.* **A 462** (2001) 152 [INSPIRE].

[24] GEANT4 collaboration, S. Agostinelli et al., *GEANT4: a simulation toolkit*, *Nucl. Instrum. Meth.* **A 506** (2003) 250 [INSPIRE].

[25] W.D. Hulsbergen, *Decay chain fitting with a Kalman filter*, *Nucl. Instrum. Meth.* **A 552** (2005) 566 [physics/0503191] [INSPIRE].

JHEP06(2012)141

[26] T. Skwarnicki, *A study of the radiative cascade transitions between the Υ' and Υ resonances*, Ph.D. thesis, Institute of Nuclear Physics, Krakow, Poland (1986) [DESY-F31-86-02].

[27] BABAR collaboration, J. Lees et al., *Branching fraction measurements of the color-suppressed decays $\bar{B}^0 \to D^{(*)0}\pi^0$, $D^{(*)0}\eta$, $D^{(*)0}\omega$ and $D^{(*)0}\eta'$ and measurement of the polarization in the decay $\bar{B}^0 \to D*0\omega$*, *Phys. Rev.* **D 84** (2011) 112007 [arXiv:1107.5751] [INSPIRE].

[28] P.J. Bickel and L. Breiman, *Sums of functions of nearest neighbor distances, moment bounds, limit theorems and a goodness of fit test*, *Ann. Prob.* **11** (1983) 185.

[29] M. Williams, *How good are your fits? Unbinned multivariate goodness-of-fit tests in high energy physics*, 2010 *JINST* **5** P09004 [arXiv:1006.3019] [INSPIRE].

[30] LHCb RICH collaboration, A. Powell, *Reconstruction and PID performance of the LHCb RICH detectors*, *Nucl. Instrum. Meth.* **A 639** (2011) 260 [INSPIRE].

[31] A. Powell et al., *Particle identification at LHCb*, PoS(ICHEP2010)020 [LHCb-PROC-2011-008].

[32] LHCb collaboration, R. Aaij et al., *Prompt K^0_S production in pp collisions at $\sqrt{s} = 0.9$ TeV*, *Phys. Lett.* **B 693** (2010) 69 [arXiv:1008.3105] [INSPIRE].

[33] M. Pivk and F.R. Le Diberder, *SPlot: a statistical tool to unfold data distributions*, *Nucl. Instrum. Meth.* **A 555** (2005) 356 [physics/0402083] [INSPIRE].

[34] Particle Data Group collaboration, K. Nakamura et al., *Review of particle physics*, *J. Phys.* **G 37** (2010) 075021 [INSPIRE].

[35] S. van der Meer, *Calibration of the effective beam height in the ISR*, ISR-PO/68-31 (1968).

[36] M. Ferro-Luzzi, *Proposal for an absolute luminosity determination in colliding beam experiments using vertex detection of beam-gas interactions*, *Nucl. Instrum. Meth.* **A 553** (2005) 388 [INSPIRE].

[37] LHCb collaboration, R. Aaij et al., *Absolute luminosity measurements with the LHCb detector at the LHC*, 2012 *JINST* **7** P01010 [arXiv:1110.2866] [INSPIRE].

[38] E. Norrbin and T. Sjöstrand, *Production and hadronization of heavy quarks*, *Eur. Phys. J.* **C 17** (2000) 137 [hep-ph/0005110] [INSPIRE].

[39] S. Alekhin, *Parton distributions from deep inelastic scattering data*, *Phys. Rev.* **D 68** (2003) 014002 [hep-ph/0211096] [INSPIRE].

JHEP06(2012)141

The LHCb collaboration

R. Aaij[38], C. Abellan Beteta[33,n], B. Adeva[34], M. Adinolfi[43], C. Adrover[6], A. Affolder[49], Z. Ajaltouni[5], J. Albrecht[35], F. Alessio[35], M. Alexander[48], S. Ali[38], G. Alkhazov[27], P. Alvarez Cartelle[34], A.A. Alves Jr[22], S. Amato[2], Y. Amhis[36], J. Anderson[37], R.B. Appleby[51], O. Aquines Gutierrez[10], F. Archilli[18,35], A. Artamonov [32], M. Artuso[53,35], E. Aslanides[6], G. Auriemma[22,m], S. Bachmann[11], J.J. Back[45], V. Balagura[28,35], W. Baldini[16], R.J. Barlow[51], C. Barschel[35], S. Barsuk[7], W. Barter[44], A. Bates[48], C. Bauer[10], Th. Bauer[38], A. Bay[36], I. Bediaga[1], S. Belogurov[28], K. Belous[32], I. Belyaev[28], E. Ben-Haim[8], M. Benayoun[8], G. Bencivenni[18], S. Benson[47], J. Benton[43], R. Bernet[37], M.-O. Bettler[17], M. van Beuzekom[38], A. Bien[11], S. Bifani[12], T. Bird[51], A. Bizzeti[17,h], P.M. Bjørnstad[51], T. Blake[35], F. Blanc[36], C. Blanks[50], J. Blouw[11], S. Blusk[53], A. Bobrov[31], V. Bocci[22], A. Bondar[31], N. Bondar[27], W. Bonivento[15], S. Borghi[48,51], A. Borgia[53], T.J.V. Bowcock[49], C. Bozzi[16], T. Brambach[9], J. van den Brand[39], J. Bressieux[36], D. Brett[51], M. Britsch[10], T. Britton[53], N.H. Brook[43], H. Brown[49], K. de Bruyn[38], A. Büchler-Germann[37], I. Burducea[26], A. Bursche[37], J. Buytaert[35], S. Cadeddu[15], O. Callot[7], M. Calvi[20,j], M. Calvo Gomez[33,n], A. Camboni[33], P. Campana[18,35], A. Carbone[14], G. Carboni[21,k], R. Cardinale[19,i,35], A. Cardini[15], L. Carson[50], K. Carvalho Akiba[2], G. Casse[49], M. Cattaneo[35], Ch. Cauet[9], M. Charles[52], Ph. Charpentier[35], N. Chiapolini[37], K. Ciba[35], X. Cid Vidal[34], G. Ciezarek[50], P.E.L. Clarke[47,35], M. Clemencic[35], H.V. Cliff[44], J. Closier[35], C. Coca[26], V. Coco[38], J. Cogan[6], P. Collins[35], A. Comerma-Montells[33], A. Contu[52], A. Cook[43], M. Coombes[43], G. Corti[35], B. Couturier[35], G.A. Cowan[36], R. Currie[47], C. D'Ambrosio[35], P. David[8], P.N.Y. David[38], I. De Bonis[4], S. De Capua[21,k], M. De Cian[37], J.M. De Miranda[1], L. De Paula[2], P. De Simone[18], D. Decamp[4], M. Deckenhoff[9], H. Degaudenzi[36,35], L. Del Buono[8], C. Deplano[15], D. Derkach[14,35], O. Deschamps[5], F. Dettori[39], J. Dickens[44], H. Dijkstra[35], P. Diniz Batista[1], F. Domingo Bonal[33,n], S. Donleavy[49], F. Dordei[11], A. Dosil Suárez[34], D. Dossett[45], A. Dovbnya[40], F. Dupertuis[36], R. Dzhelyadin[32], A. Dziurda[23], S. Easo[46], U. Egede[50], V. Egorychev[28], S. Eidelman[31], D. van Eijk[38], F. Eisele[11], S. Eisenhardt[47], R. Ekelhof[9], L. Eklund[48], Ch. Elsasser[37], D. Elsby[42], D. Esperante Pereira[34], A. Falabella[16,e,14], C. Färber[11], G. Fardell[47], C. Farinelli[38], S. Farry[12], V. Fave[36], V. Fernandez Albor[34], M. Ferro-Luzzi[35], S. Filippov[30], C. Fitzpatrick[47], M. Fontana[10], F. Fontanelli[19,i], R. Forty[35], O. Francisco[2], M. Frank[35], C. Frei[35], M. Frosini[17,f], S. Furcas[20], A. Gallas Torreira[34], D. Galli[14,c], M. Gandelman[2], P. Gandini[52], Y. Gao[3], J-C. Garnier[35], J. Garofoli[53], J. Garra Tico[44], L. Garrido[33], D. Gascon[33], C. Gaspar[35], R. Gauld[52], N. Gauvin[36], M. Gersabeck[35], T. Gershon[45,35], Ph. Ghez[4], V. Gibson[44], V.V. Gligorov[35], C. Göbel[54], D. Golubkov[28], A. Golutvin[50,28,35], A. Gomes[2], H. Gordon[52], M. Grabalosa Gándara[33], R. Graciani Diaz[33], L.A. Granado Cardoso[35], E. Graugés[33], G. Graziani[17], A. Grecu[26], E. Greening[52], S. Gregson[44], B. Gui[53], E. Gushchin[30], Yu. Guz[32], T. Gys[35], C. Hadjivasiliou[53], G. Haefeli[36], C. Haen[35], S.C. Haines[44], T. Hampson[43], S. Hansmann-Menzemer[11], R. Harji[50], N. Harnew[52], J. Harrison[51], P.F. Harrison[45], T. Hartmann[55], J. He[7], V. Heijne[38], K. Hennessy[49], P. Henrard[5], J.A. Hernando Morata[34], E. van Herwijnen[35], E. Hicks[49], K. Holubyev[11],

JHEP06(2012)141

P. Hopchev[4], W. Hulsbergen[38], P. Hunt[52], T. Huse[49], R.S. Huston[12], D. Hutchcroft[49], D. Hynds[48], V. Iakovenko[41], P. Ilten[12], J. Imong[43], R. Jacobsson[35], A. Jaeger[11], M. Jahjah Hussein[5], E. Jans[38], F. Jansen[38], P. Jaton[36], B. Jean-Marie[7], F. Jing[3], M. John[52], D. Johnson[52], C.R. Jones[44], B. Jost[35], M. Kaballo[9], S. Kandybei[40], M. Karacson[35], T.M. Karbach[9], J. Keaveney[12], I.R. Kenyon[42], U. Kerzel[35], T. Ketel[39], A. Keune[36], B. Khanji[6], Y.M. Kim[47], M. Knecht[36], R.F. Koopman[39], P. Koppenburg[38], M. Korolev[29], A. Kozlinskiy[38], L. Kravchuk[30], K. Kreplin[11], M. Kreps[45], G. Krocker[11], P. Krokovny[11], F. Kruse[9], K. Kruzelecki[35], M. Kucharczyk[20,23,35,j], V. Kudryavtsev[31], T. Kvaratskheliya[28,35], V.N. La Thi[36], D. Lacarrere[35], G. Lafferty[51], A. Lai[15], D. Lambert[47], R.W. Lambert[39], E. Lanciotti[35], G. Lanfranchi[18], C. Langenbruch[11], T. Latham[45], C. Lazzeroni[42], R. Le Gac[6], J. van Leerdam[38], J.-P. Lees[4], R. Lefèvre[5], A. Leflat[29,35], J. Lefrançois[7], O. Leroy[6], T. Lesiak[23], L. Li[3], L. Li Gioi[5], M. Lieng[9], M. Liles[49], R. Lindner[35], C. Linn[11], B. Liu[3], G. Liu[35], J. von Loeben[20], J.H. Lopes[2], E. Lopez Asamar[33], N. Lopez-March[36], H. Lu[3], J. Luisier[36], A. Mac Raighne[48], F. Machefert[7], I.V. Machikhiliyan[4,28], F. Maciuc[10], O. Maev[27,35], J. Magnin[1], S. Malde[52], R.M.D. Mamunur[35], G. Manca[15,d], G. Mancinelli[6], N. Mangiafave[44], U. Marconi[14], R. Märki[36], J. Marks[11], G. Martellotti[22], A. Martens[8], L. Martin[52], A. Martín Sánchez[7], M. Martinelli[38], D. Martinez Santos[35], A. Massafferri[1], Z. Mathe[12], C. Matteuzzi[20], M. Matveev[27], E. Maurice[6], B. Maynard[53], A. Mazurov[16,30,35], G. McGregor[51], R. McNulty[12], M. Meissner[11], M. Merk[38], J. Merkel[9], S. Miglioranzi[35], D.A. Milanes[13], M.-N. Minard[4], J. Molina Rodriguez[54], S. Monteil[5], D. Moran[12], P. Morawski[23], R. Mountain[53], I. Mous[38], F. Muheim[47], K. Müller[37], R. Muresan[26], B. Muryn[24], B. Muster[36], J. Mylroie-Smith[49], P. Naik[43], T. Nakada[36], R. Nandakumar[46], I. Nasteva[1], M. Needham[47], N. Neufeld[35], A.D. Nguyen[36], C. Nguyen-Mau[36,o], M. Nicol[7], V. Niess[5], N. Nikitin[29], A. Nomerotski[52,35], A. Novoselov[32], A. Oblakowska-Mucha[24], V. Obraztsov[32], S. Oggero[38], S. Ogilvy[48], O. Okhrimenko[41], R. Oldeman[15,d,35], M. Orlandea[26], J.M. Otalora Goicochea[2], P. Owen[50], K. Pal[53], J. Palacios[37], A. Palano[13,b], M. Palutan[18], J. Panman[35], A. Papanestis[46], M. Pappagallo[48], C. Parkes[51], C.J. Parkinson[50], G. Passaleva[17], G.D. Patel[49], M. Patel[50], S.K. Paterson[50], G.N. Patrick[46], C. Patrignani[19,i], C. Pavel-Nicorescu[26], A. Pazos Alvarez[34], A. Pellegrino[38], G. Penso[22,l], M. Pepe Altarelli[35], S. Perazzini[14,c], D.L. Perego[20,j], E. Perez Trigo[34], A. Pérez-Calero Yzquierdo[33], P. Perret[5], M. Perrin-Terrin[6], G. Pessina[20], A. Petrolini[19,i], A. Phan[53], E. Picatoste Olloqui[33], B. Pie Valls[33], B. Pietrzyk[4], T. Pilař[45], D. Pinci[22], R. Plackett[48], S. Playfer[47], M. Plo Casasus[34], G. Polok[23], A. Poluektov[45,31], E. Polycarpo[2], D. Popov[10], B. Popovici[26], C. Potterat[33], A. Powell[52], J. Prisciandaro[36], V. Pugatch[41], A. Puig Navarro[33], W. Qian[53], J.H. Rademacker[43], B. Rakotomiaramanana[36], M.S. Rangel[2], I. Raniuk[40], G. Raven[39], S. Redford[52], M.M. Reid[45], A.C. dos Reis[1], S. Ricciardi[46], A. Richards[50], K. Rinnert[49], D.A. Roa Romero[5], P. Robbe[7], E. Rodrigues[48,51], F. Rodrigues[2], P. Rodriguez Perez[34], G.J. Rogers[44], S. Roiser[35], V. Romanovsky[32], M. Rosello[33,n], J. Rouvinet[36], T. Ruf[35], H. Ruiz[33], G. Sabatino[21,k], J.J. Saborido Silva[34], N. Sagidova[27], P. Sail[48], B. Saitta[15,d], C. Salzmann[37], M. Sannino[19,i], R. Santacesaria[22], C. Santamarina Rios[34], R. Santinelli[35], E. Santovetti[21,k], M. Sapunov[6], A. Sarti[18,l], C. Satriano[22,m], A. Satta[21], M. Savrie[16,e], D. Savrina[28], P. Schaack[50], M. Schiller[39],

JHEP06(2012)141

H. Schindler[35], S. Schleich[9], M. Schlupp[9], M. Schmelling[10], B. Schmidt[35], O. Schneider[36], A. Schopper[35], M.-H. Schune[7], R. Schwemmer[35], B. Sciascia[18], A. Sciubba[18,l], M. Seco[34], A. Semennikov[28], K. Senderowska[24], I. Sepp[50], N. Serra[37], J. Serrano[6], P. Seyfert[11], M. Shapkin[32], I. Shapoval[40,35], P. Shatalov[28], Y. Shcheglov[27], T. Shears[49], L. Shekhtman[31], O. Shevchenko[40], V. Shevchenko[28], A. Shires[50], R. Silva Coutinho[45], T. Skwarnicki[53], N.A. Smith[49], E. Smith[52,46], K. Sobczak[5], F.J.P. Soler[48], A. Solomin[43], F. Soomro[18,35], B. Souza De Paula[2], B. Spaan[9], A. Sparkes[47], P. Spradlin[48], F. Stagni[35], S. Stahl[11], O. Steinkamp[37], S. Stoica[26], S. Stone[53,35], B. Storaci[38], M. Straticiuc[26], U. Straumann[37], V.K. Subbiah[35], S. Swientek[9], M. Szczekowski[25], P. Szczypka[36], T. Szumlak[24], S. T'Jampens[4], E. Teodorescu[26], F. Teubert[35], C. Thomas[52], E. Thomas[35], J. van Tilburg[11], V. Tisserand[4], M. Tobin[37], S. Topp-Joergensen[52], N. Torr[52], E. Tournefier[4,50], S. Tourneur[36], M.T. Tran[36], A. Tsaregorodtsev[6], N. Tuning[38], M. Ubeda Garcia[35], A. Ukleja[25], U. Uwer[11], V. Vagnoni[14], G. Valenti[14], R. Vazquez Gomez[33], P. Vazquez Regueiro[34], S. Vecchi[16], J.J. Velthuis[43], M. Veltri[17,g], B. Viaud[7], I. Videau[7], D. Vieira[2], X. Vilasis-Cardona[33,n], J. Visniakov[34], A. Vollhardt[37], D. Volyanskyy[10], D. Voong[43], A. Vorobyev[27], H. Voss[10], R. Waldi[55], S. Wandernoth[11], J. Wang[53], D.R. Ward[44], N.K. Watson[42], A.D. Webber[51], D. Websdale[50], M. Whitehead[45], D. Wiedner[11], L. Wiggers[38], G. Wilkinson[52], M.P. Williams[45,46], M. Williams[50], F.F. Wilson[46], J. Wishahi[9], M. Witek[23], W. Witzeling[35], S.A. Wotton[44], K. Wyllie[35], Y. Xie[47], F. Xing[52], Z. Xing[53], Z. Yang[3], R. Young[47], O. Yushchenko[32], M. Zangoli[14], M. Zavertyaev[10,a], F. Zhang[3], L. Zhang[53], W.C. Zhang[12], Y. Zhang[3], A. Zhelezov[11], L. Zhong[3] and A. Zvyagin[35]

[1]: Centro Brasileiro de Pesquisas Físicas (CBPF), Rio de Janeiro, Brazil
[2]: Universidade Federal do Rio de Janeiro (UFRJ), Rio de Janeiro, Brazil
[3]: Center for High Energy Physics, Tsinghua University, Beijing, China
[4]: LAPP, Université de Savoie, CNRS/IN2P3, Annecy-Le-Vieux, France
[5]: Clermont Université, Université Blaise Pascal, CNRS/IN2P3, LPC, Clermont-Ferrand, France
[6]: CPPM, Aix-Marseille Université, CNRS/IN2P3, Marseille, France
[7]: LAL, Université Paris-Sud, CNRS/IN2P3, Orsay, France
[8]: LPNHE, Université Pierre et Marie Curie, Université Paris Diderot, CNRS/IN2P3, Paris, France
[9]: Fakultät Physik, Technische Universität Dortmund, Dortmund, Germany
[10]: Max-Planck-Institut für Kernphysik (MPIK), Heidelberg, Germany
[11]: Physikalisches Institut, Ruprecht-Karls-Universität Heidelberg, Heidelberg, Germany
[12]: School of Physics, University College Dublin, Dublin, Ireland
[13]: Sezione INFN di Bari, Bari, Italy
[14]: Sezione INFN di Bologna, Bologna, Italy
[15]: Sezione INFN di Cagliari, Cagliari, Italy
[16]: Sezione INFN di Ferrara, Ferrara, Italy
[17]: Sezione INFN di Firenze, Firenze, Italy
[18]: Laboratori Nazionali dell'INFN di Frascati, Frascati, Italy
[19]: Sezione INFN di Genova, Genova, Italy
[20]: Sezione INFN di Milano Bicocca, Milano, Italy

JHEP06(2012)141

[21]: Sezione INFN di Roma Tor Vergata, Roma, Italy
[22]: Sezione INFN di Roma La Sapienza, Roma, Italy
[23]: Henryk Niewodniczanski Institute of Nuclear Physics Polish Academy of Sciences, Kraków, Poland
[24]: AGH University of Science and Technology, Kraków, Poland
[25]: Soltan Institute for Nuclear Studies, Warsaw, Poland
[26]: Horia Hulubei National Institute of Physics and Nuclear Engineering, Bucharest-Magurele, Romania
[27]: Petersburg Nuclear Physics Institute (PNPI), Gatchina, Russia
[28]: Institute of Theoretical and Experimental Physics (ITEP), Moscow, Russia
[29]: Institute of Nuclear Physics, Moscow State University (SINP MSU), Moscow, Russia
[30]: Institute for Nuclear Research of the Russian Academy of Sciences (INR RAN), Moscow, Russia
[31]: Budker Institute of Nuclear Physics (SB RAS) and Novosibirsk State University, Novosibirsk, Russia
[32]: Institute for High Energy Physics (IHEP), Protvino, Russia
[33]: Universitat de Barcelona, Barcelona, Spain
[34]: Universidad de Santiago de Compostela, Santiago de Compostela, Spain
[35]: European Organization for Nuclear Research (CERN), Geneva, Switzerland
[36]: Ecole Polytechnique Fédérale de Lausanne (EPFL), Lausanne, Switzerland
[37]: Physik-Institut, Universität Zürich, Zürich, Switzerland
[38]: Nikhef National Institute for Subatomic Physics, Amsterdam, The Netherlands
[39]: Nikhef National Institute for Subatomic Physics and Vrije Universiteit, Amsterdam, The Netherlands
[40]: NSC Kharkiv Institute of Physics and Technology (NSC KIPT), Kharkiv, Ukraine
[41]: Institute for Nuclear Research of the National Academy of Sciences (KINR), Kyiv, Ukraine
[42]: University of Birmingham, Birmingham, United Kingdom
[43]: H.H. Wills Physics Laboratory, University of Bristol, Bristol, United Kingdom
[44]: Cavendish Laboratory, University of Cambridge, Cambridge, United Kingdom
[45]: Department of Physics, University of Warwick, Coventry, United Kingdom
[46]: STFC Rutherford Appleton Laboratory, Didcot, United Kingdom
[47]: School of Physics and Astronomy, University of Edinburgh, Edinburgh, United Kingdom
[48]: School of Physics and Astronomy, University of Glasgow, Glasgow, United Kingdom
[49]: Oliver Lodge Laboratory, University of Liverpool, Liverpool, United Kingdom
[50]: Imperial College London, London, United Kingdom
[51]: School of Physics and Astronomy, University of Manchester, Manchester, United Kingdom
[52]: Department of Physics, University of Oxford, Oxford, United Kingdom
[53]: Syracuse University, Syracuse, NY, United States
[54]: Pontifícia Universidade Católica do Rio de Janeiro (PUC-Rio), Rio de Janeiro, Brazil, associated to [2]:]
[55]: Physikalisches Institut, Universität Rostock, Rostock, Germany, associated to [11]:]

[a]: P.N. Lebedev Physical Institute, Russian Academy of Science (LPI RAS), Moscow, Russia
[b]: Università di Bari, Bari, Italy
[c]: Università di Bologna, Bologna, Italy
[d]: Università di Cagliari, Cagliari, Italy
[e]: Università di Ferrara, Ferrara, Italy
[f]: Università di Firenze, Firenze, Italy

JHEP06(2012)141

[g]: Università di Urbino, Urbino, Italy
[h]: Università di Modena e Reggio Emilia, Modena, Italy
[i]: Università di Genova, Genova, Italy
[j]: Università di Milano Bicocca, Milano, Italy
[k]: Università di Roma Tor Vergata, Roma, Italy
[l]: Università di Roma La Sapienza, Roma, Italy
[m]: Università della Basilicata, Potenza, Italy
[n]: LIFAELS, La Salle, Universitat Ramon Llull, Barcelona, Spain
[o]: Hanoi University of Science, Hanoi, Viet Nam

JHEP06(2012)141